Fall 12-17-2019

Structural and Geochronologic Constraints on the Duration of the Picuris Orogeny and Demise of an Orogenic Plateau, northern NM

Daniel J. Young
University of New Mexico - Main Campus

Daniel J. Young

Candidate

Earth and Planetary Sciences

Department

This thesis is approved, and it is acceptable in quality and form for publication:

Approved by the Thesis Committee:

Dr. Karl E. Karlstrom , Chairperson

Dr. Adrian Brearley

Dr. Matthew Heizler

Structural and Geochronologic Constraints on the Duration of the Picuris Orogeny and Demise of an Orogenic Plateau, northern NM

BY

DANIEL J. YOUNG

B.S., General Geology,
The University of Texas at Austin, 2017

THESIS

Submitted in Partial Fulfillment of the
Requirements for the Degree of

Master of Science

Earth and Planetary Science

The University of New Mexico
Albuquerque, New Mexico

May, 2020

ACKNOWLEDGEMENTS

I would like to first thank Karl Karlstrom for his unyielding efforts to encourage and assist me in the time spent working on this body of research. I could not ask for a more involved advisor in the field and in the office. Wherever I may land professionally I will always recall his drive and unending enthusiasm in his work as a guiding light. Without him this body of research would not have been possible to produce. Secondly, I need to thank collaborators Matthew Heizler and Mike Williams for their time spent completing the bulk of the geochronology work presented here. Their patience and willingness to complete the analyses on these samples leaves me indebted to them. Adrian Brearley also deserves thanks for his role on my committee and valuable petrologic insights.

Lastly, in an effort to leave no one out, I owe thanks to the following people/groups/animals for their intellectual and emotional support during my master's degree, be it in the field, office, home, or elsewhere: Jacob Thacker, Micael Albonico, Jordan Anderson, Carmen Winn, Christina Ferguson, Mark Holland, Cory Walk, Ben Holt, Jeff Hrncir, Jon Golla, Laura Crossey, Spencer Staley, Zach Gallegos, Brad Jeffreys, Zoltan Vaci, Rose Hurlow, Remy Rovelli, Camille Dwyer, Jessica Johnson, Justin Wilgus, Katie Holleron, Chris Bayer, Mya Habermann, Colleen Nilan, Marcus Albonico, Chris Eason, Jennifer Imbrogno, Carly Zuniga, Nick Kantor, Erin Farrar, Rachel Ruthven, Dylan de la Garza, Aaron and Danni, Mom, Dad, Sister, Brother, the Hoodoos, Grubbs, Gato, Orange Puff Puff, Spyro, Skippy, Pudge, Lucky, Molly, Lily, and Shoni.

Structural and Geochronologic Constraints on the Duration of the Picuris Orogeny and Demise of an Orogenic Plateau, northern NM

By

DANIEL J. YOUNG

Bachelor of Science, General Geology

Master of Science, Earth and Planetary Science

ABSTRACT

Metasedimentary and igneous basement rocks in northern New Mexico record episodic pulses of tectonism during cratonic growth from 1.8 to 1.38 Ga. Continued challenges involve parsing the deformational features attributable to the Yavapai Orogeny (1.71-1.68 Ga), Mazatzal orogeny (1.66-1.60 Ga), and Picuris orogeny (1.5-1.38 Ga) in this region and understanding how older structures may have been overprinted and reactivated to explain the observed strain. This paper presents regional cross-sections of the 1.7 Ga Vadito, 1.68 to 1.50 Ga Hondo, and 1.5-1.45 Ga Trampas groups of the Picuris Mountains and Rio Mora areas of northern New Mexico combined with new geochronologic and thermochronologic constraints. These data suggest the following tectonic evolution. An early bedding-parallel S1 fabric is present only in pre-Trampas Group rocks and is interpreted to be related to early isoclinal folds and thrusts. All groups were folded by F2 and F3 fold generations during the Picuris orogeny. New U-Pb dates from monazite cores of about 1.5 Ga in aluminous gneisses from the Vadito- Hondo group aluminous contact zone within the Pecos thrust sheet are interpreted as onset of Picuris orogeny prograde tectonism. This onset of heating/deformation is thus close in

age, and apparently pre-dates deposition of the Trampas Group at ~1488 ± 6 Ma in the footwall of the Pecos and Plomo thrusts. Growth of metamorphic garnets at 1.45- 1.40 Ga from previous studies and new monazite rim dates of ~1.45 Ga may record metamorphism close in age to deposition of the thrust-bound 1.453 ± 10 Ga Marqueñas Formation.

Regional cross sections show that the modern surface exposure represents an exhumed ~ 15 km middle crustal duplex system that juxtaposes, from north to south: 1) 1.45 Ga triple point (>550 C, 3.5 kbars) polyphase metamorphic tectonites in the Copper Hill anticline- Hondo syncline thrust sheet made between the Pilar and Plomo thrusts, 2) a similar grade thrust-bound Marquenas tectonite that makes up the Plomo shear zone, 3) the 1.45 Ga Penasco granite that intrudes Vadito Group rocks between the Plomo shear zone and the Pecos master thrust, and 4) overriding volcanic rocks of the ~ 1.72-1.65 Ga Pecos volcanic complex. Juxtaposition of amphibolite-grade upper plate rocks against 1.48-1.45 Ga metasedimentary lower plate rocks as the product of progressive thrusting from 1.50 to 1.40 Ga synchronous with development of syntectonic foreland basins. The 1.45 Ga granite and pegmatites show only minor penetrative strain but are considered broadly syntectonic with waning deformation at 1.45- 1.40 Ga. A modern analog is the Tien Shan – Tarim basin region of the interior Tibetan Plateau inferred for the Picuris tectonism.

New $^{40}Ar/^{39}Ar$ dates on hornblende and muscovite constrain cooling through ~500 °C and ~350-400 °C respectively and provide insight into cooling rates following the Picuris orogeny, and hence the nature and timing of demise of Picuris orogenic uplifts. Hondo and Trampas group rocks cooled through 500 °C 1420-1381 Ma and

through 350 °C from 1378-1359 Ma. This is similar to new data with $^{40}Ar/^{39}Ar$ cooling data from muscovite from the Petaca pegmatite district (mean cooling age of 1375 ± 10 Ma), and similar ages in basement exposures from neighboring mountain ranges. Slow cooling from >500 to <350 °C from ~1420 to ~1360 Ma suggests cooling rates of ~ 3 °C/Ma over 60 Ma following peak triple point metamorphism. To explain this protracted cooling we propose that an orogenic plateau was built by thrust duplexing and penetrative folding in northern New Mexico during the Picuris orogeny followed by relatively slow erosional removal. Erosion of much of the region initiated by 1.1-1.3 Ga, resulting in deposition of the Debaca Group and correlative strata.

TABLE OF CONTENTS

LIST OF FIGURES

LIST OF APPENDICES

Introduction

The southern margin of Laurentia has been viewed in terms of the southward growth of continental lithosphere by addition of juvenile terranes along a long-lived contractional margin that persisted from 1.8 to 1.0 Ga (Karlstrom et al., 2001). As shown in Figure 1, south-younging crustal provinces include the 1.8-1.7 Ga Yavapai province, 1.7-1.6 Ga Mazatzal province, and 1.5-1.4 Granite Rhyolite crustal age provinces; these

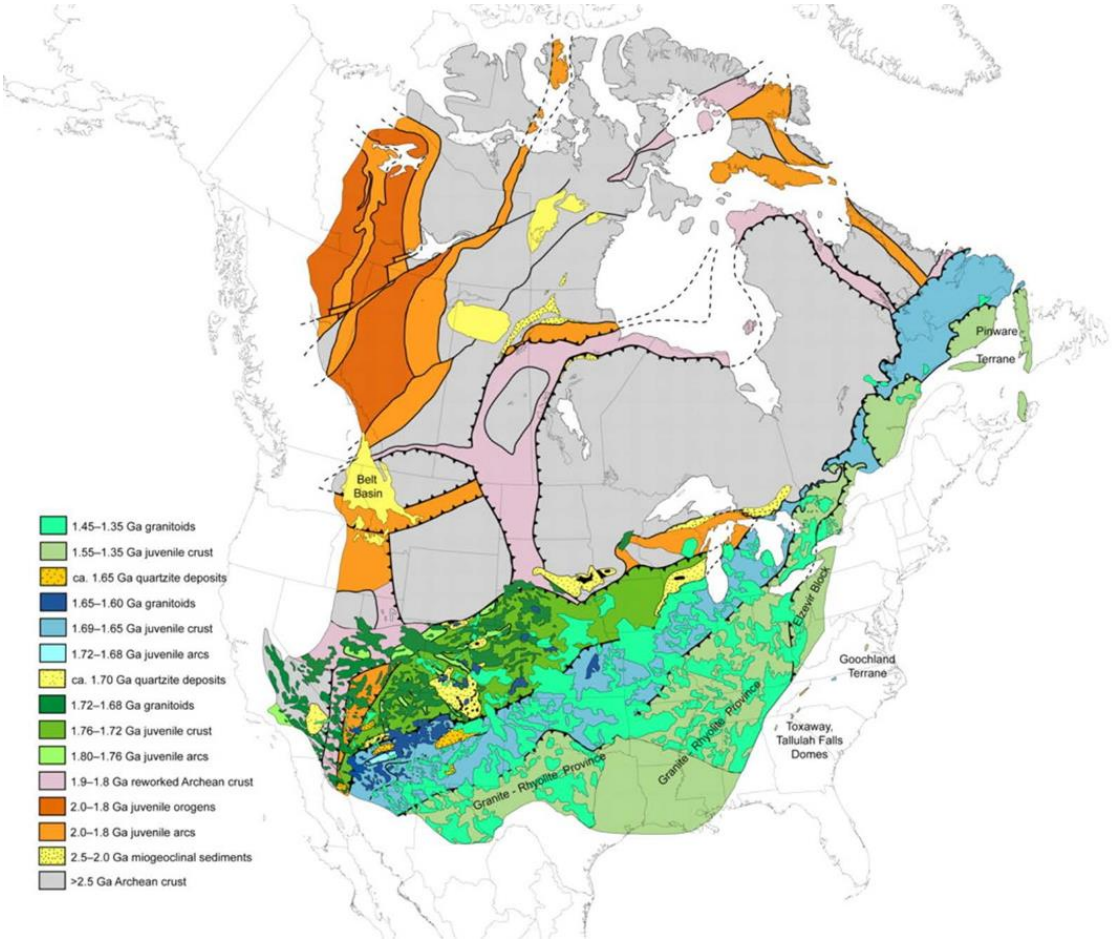

Figure 1: Time slice of North American accretion at ~1.45 Ga, taken from Whitmeyer and Karlstrom (2007) showing 1.48-1.35 Ga A-type granites (light green) stitching the Granite-Rhyolite, Mazatzal, and Yavapai provinces along the southern (present-day orientation) Laurentian margin. The plutons were inferred in part from North American Magnetic Anomaly Group, 2002

were assembled during proposed accretionary polyphase tectonism in the Yavapai (1.75-

1.7 Ga), Mazatzal (1.65-1.6 Ga), and Picuris (1.5-1.40 Ga) orogenies (Whitmeyer and Karlstrom, 2007; Daniel et al., 2013; Karlstrom et al., 2015). The location of the study area in the following work is in northern New Mexico, along the traditional Yavapai-Mazatzal crustal province boundary and in an area of especially intense tectonism during the Picuris orogeny.

Recent work re-dating sedimentary units in Precambrian exposures in the Picuris Mountains has revitalized research on the tectonic significance and history of the different orogenies along the modern-day southwestern Laurentian margin (Jones et al., 2011; Doe et al., 2012; Daniel et al., 2013; Bickford et al., 2015; Karlstrom et al., 2015; Marshall et al., 2017). This has led to new questions concerning the timing and nature of metamorphism and deformation and to new models of orogenesis along the Laurentian margin (Daniel et al., 2013; Karlstrom et al., 2015). In

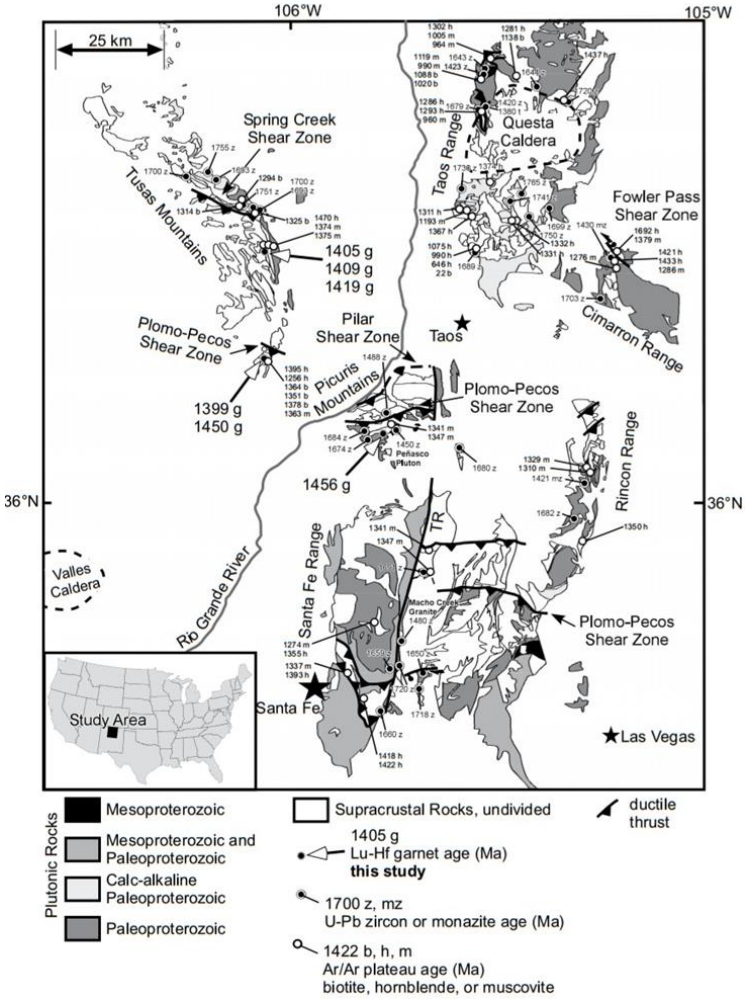

Figure 2: Map of dated metamorphic and igneous minerals in the southern Rocky Mountains of northern NM. Shown are Lu-Hf garnet ages, U-Pb zircon and monazite ages, and $^{40}Ar/^{39}Ar$ plateau ages for biotite, muscovite, and hornblende. Only Precambrian rocks are mapped. Taken from Aronoff et al., 2016.

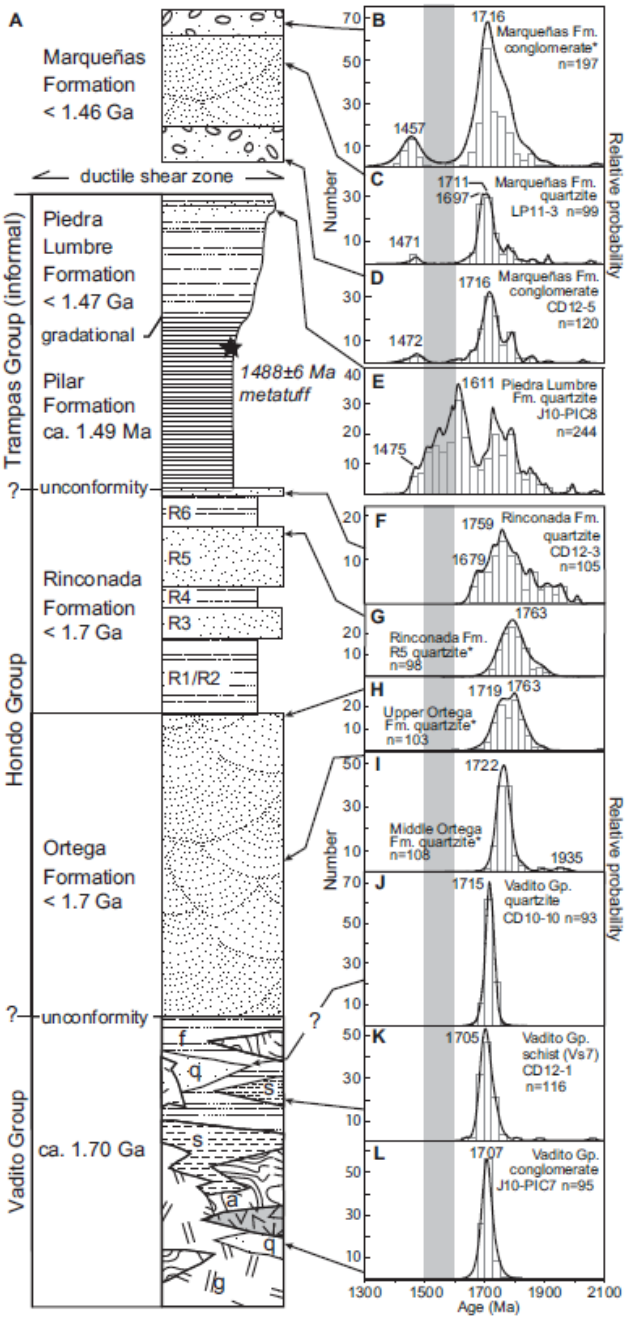

Figure 3. Stratigraphic sequence of the Precambrian rocks of the Picuris area. B-L show 207U/206U age probability diagrams for detrital zircons., with asterisked plots being from Jones et al., 2011 and unasterisked plots being from Daniel et al., 2013. Taken from Daniel et al., 2013.

particular, the discovery of the 1.50-1.45 Ga Trampas Group (Daniel et al., 2013) and correlatives in Arizona (Doe et al., 2012) now offers a powerful new tool for identifying pre- versus post-Trampas Group strain (Mako et al., 2014). The goal of this paper is to present additional work on the nature of contacts between 1.48 Ga metasedimentary rocks and older rocks in northern New Mexico and offer new $^{40}Ar/^{39}Ar$ thermochronology and U-Pb-Th petrochronology in an effort to better understand the tectonic evolution of this region.

Figure 2 shows the study area and Figure 3 shows the main tectonostratigraphic units of northern New Mexico. The basement units are the >1.76 Ga Mopin Series, an older volcanogenic arc succession. They are overlain by the 1.71-1.70 Ga Vadito

Group, a succession of volcanic and volcaniclastic rocks, including 1.7 Ga rhyolites. The ≤1.67 Ga Hondo Group overlies the Vadito Group gradationally and consists of the 1-2 km-thick Ortega Quartzite. The 1.5-1.45 Ga Trampas Group overlies the Hondo Group and consists of 1.48-1.45 Ga graphitic slates and the ≤1.45 conglomerates of the Marqueñas Formation. The age of the Hondo Group is not yet well known, but its maximum depositional age from detrital zircons is 1670 ±3 Ma and it is overlain unconformably by the Trampas Group. Part of this time period was also within a proposed 1.6-1.5 Ga gap in magmatism and tectonism in New Mexico (Karlstrom et al., 2005). But the position of unconformities and the tectonic evolution within the 1.7-1.5 Ga time interval remain incompletely understood major research questions.

This paper has three parts. 1) We conducted a field and structural study of the nature of the contact between the Hondo and Trampas groups of northern New Mexico to test the nature of this contat. 2) We present new geochronologic and thermochronologic data from several of the structural packages to evaluate tectonic history. 3) We compile and synthesize magmatic and metamorphic data from previous workers on the 1.5-1.4 Ga Picuris orogeny and 1.65- 1.60 Ga Mazatzal tectonism to help distinguish the history and different expressions of these two orogenies.

Previous work

The tectonism associated with the 1.5-1.4 Ga Picuris orogeny that is the focus of this study is preceded by a 1.68-1.60 Ga period of continental arc magmatism and arc and backarc basin formation (e.g the Manzano Group), generation of juvenile crust (in part), and subsequent 1.65-1.60 Ga northwest-vergent shortening of the Manzano thrust belt with syntectonic pluton emplacement known as the Mazatzal orogeny (Whitmeyer and

Karlstrom, 2007). This event extends spatially from Arizona across southern Laurentia to the Canadian Maritime provinces, equivalent with the Labradorian crustal province as shown in Figure 1. In the Southwest this crustal province covers much of central and southeastern Arizona, central and southern New Mexico, and northern Chihuahua and Sonora (Whitmeyer and Karlstrom, 2007). Supercrustal metavolcanics rocks grade upward into variably deformed metasedimentary successions that extend across this region (Amato, 2009; Doe et al., 2012; Mako et al., 2014; Duebendorfer et al., 2015). Generally, the base of the Manzano Group and correlative successions consists of 1.70-1.66 Ga metarhyolites and generally coeval calc-alkaline intrusions that are indicative of regional arc magmatism. These plutons and their metasedimentary contact aureoles make up the majority of exposed rock in this province (Whitmeyer and Karlstrom, 2007; Duebendorfer et al., 2015). Recent work in the Picuris and Four Corners area of Arizona has redated what was before considered Mazatzal-aged sedimentary rocks to be Mesoproterozoic in age, leading some workers to question the spatial extent and magnitude, even the existence, of the Mazatzal orogeny (Jones et al., 2011; Doe et al., 2012; Daniel et al., 2013; Mako et al., 2014) whereas other workers continue to document 1.65-1.60 Ga tectonism in the region (Amato, 2009; Karlstrom et al., 2016). This work is intended to further test and clarify the nature of polyphase tectonism in northern New Mexico.

Throughout much of the Southwest, following cessation of 1.65-1.60 plutonism, sedimentation, and potential deformation, there was a lack of tectonic activity from 1.6-1.5 Ga. This lull in deformation, magmatism, and general development of crust in southern Laurentia is referred to as the “tectonic gap” (Karlstrom et al., 2004;

Duebendorfer et al., 2006; Doe et al., 2012) and could have led to development of an unconformity between Paleoproterozoic and Mesoproterozoic rocks. In northern New Mexico, this time gap extends for 200 Ma between the 1.70 Ga Vadito Group and the 1.5 Ga Trampas Groups, but the age of the intervening Hondo Group is uncertain. Filling in this tectonic gap has been a longtime goal of researchers. The upper Hess Canyon Group of Arizona was also redated at 1488 ±9 Ma, containing zircon dates of 1.6-1.5 Ga tectonic gap age (Doe et al., 2012). This leads to the hypothesis that, assuming the tectonic gap was Laurentia-wide, these grains came from outboard of Laurentia, perhaps Australia (Ross and Eaton, 2002; Doe et al., 2012). Understanding the nature of the contact between the Hondo and Trampas groups in the Picuris may help us understand more about what occurred during this time in the North American Proterozoic rock record.

Overview of basement rocks of northern New Mexico

The sequence of metasedimentary and metavolcanic Precambrian rock in the Picuris and Rio Mora areas is divided into three main sequences: the Vadito Group, the Hondo Group, and the Trampas Group. Much of the dating on these sequences has been refined via U-Pb dating of detrital zircons by Jones et al. (2011) and Daniel et al. (2013) (Figure 3). The Vadito Group consists of complexly interbedded 1.71 Ga felsic metavolcanics, schists, and quartzites with pebble conglomerates that are cross-cut by 1.674 ± 5 Ma to 1.684 ± 1 Ma plutons (Bell, 1985; Bauer, 1993; Daniel et al., 2013; Whitmeyer and Karlstrom, 2007). The 2-km-thick Hondo Group gradationally overlies the Vadito Group (Bauer, 1993) and hence has been assumed to be 1.7 Ga at its base (Daniel et al., 2013). The schists and quartzites of the Rinconada Formation have not

been directly dated but are presently assigned to the upper Hondo Group. The 1.5-km-thick Ortega Formation consists of multiple packages of ultra-mature aluminous quartzites with well-preserved crossbeds, and as shown in Figure 3, has a narrow, unimodal detrital zircon age peak of 1,715-1,763 Ma that broadens to ~1.80-1.68 Ga up section, perhaps suggesting more varied and distal source regions. The unimodal detrital zircon signature of the Ortega Formation is typical of Paleoproterozoic quartzite sequences in the southwest (Bauer and Williams, 1989; Jones et al., 2011; Daniel et al., 2013). The Rinconada Formation, one of the targets of this study, consists of a series of 6 interbedded quartzite and schist packages that have a maximum depositional ages of 1679 ± 18 Ma based on detrital zircon studies (Daniel et al., 2013).

The Pilar Formation marks the beginning of the Trampas Group and consists of interbedded phyllite and metatuff, with the overlying Piedra Lumbre phyllite (Bauer and Williams, 1989). Daniel et al. (2013) dated zircon in a metatuff layer from the Pilar and determined a depositional age of 1488 ± 6 Ma. This new evidence leads researchers to infer that the contact between the Trampas and Hondo Groups could represent a major unconformity (Daniel et al., 2013; Jones et al., 2011). This implies that a ~100 Ma tectonic gap may exist between the Mesoproterozoic Trampas Group and the Paleoproterozoic Hondo Group. The nature of this unconformity has yet to be investigated in detail, and what geologic events took place during this tectonic gap is a topic of discussion in the literature (e.g., Doe et al., 2012). For example, it is unknown if it represents an angular unconformity separating different periods of tectonism, or if the contact is conformable between the Hondo and Trampas groups, with the major time break lower in the section, between the Vadito and Hondo groups. If the Hondo-Trampas

group contact is an angular unconformity, this contact may give us the ability to differentiate deformation caused by the Mazatzal orogeny in the Hondo and Vadito groups from deformation caused by the Picuris orogeny.

Methods

Samples DY18-RM-22, DY-18-RM-23, and DY18-RM-25 were collected during fieldwork in the Rio Mora area of the Pecos Wilderness for U-Th-Pb monazite dating via electron microprobe analysis (EPMA) at the University of Massachusetts Amherst following the methods of Williams et al. (2006; 2007). Thirty micron thick polished thin sections of each sample were first microstructurally analyzed in a polarizing optical microscope, looking for kinematic indicators and characterizing the aluminosilicate growth in each sample. These thin sections then underwent wavelength dispersive spectroscopy (WDS) compositional mapping for Ce and La X-ray intensity on a Cameca SX-50 microprobe. Other compositional maps of U, Th, Y, Ca, and Nd were made for specific monazite grains to identify domains of monazite growth that could be independently dated.

$^{40}Ar/^{39}Ar$ analyses were done on samples from Rio Mora at the New Mexico Geochronology Research Laboratory, New Mexico Institute of Mining and Technology, using a diode laser to heat. Hornblende and muscovite separates were obtained from crushed, washed, and sieved samples by hand picking 50–100 crystals from the 60–90 mesh sieve fraction. Step heating and total fusion experiments were conducted at the beam coupled to a MAP 215-50 mass spectrometer. The step heated and total fusion ages are combined in probability distribution plots using 1 sigma uncertainties and the full analytical results are reported in Appendix 2. The $^{40}Ar/^{39}Ar$ ages derived from these

metamorphic hornblende and muscovite grains are cooling ages that reflect cooling through closure temperatures of Ar diffusion for these mineral. Closure temperatures are a function of grain size and cooling rate and range from 550 to 500 °C for hornblende and 300 to 420 °C for muscovite (Harrison, 1981; Harrison et al., 2009). We use ~ 500 °C for hornblende and ~350 °C for muscovite given the slow cooling we document in this paper.

Structural and stratigraphic analysis of the Hondo-Trampas Group contact in the Picuris Mountains , New Mexico

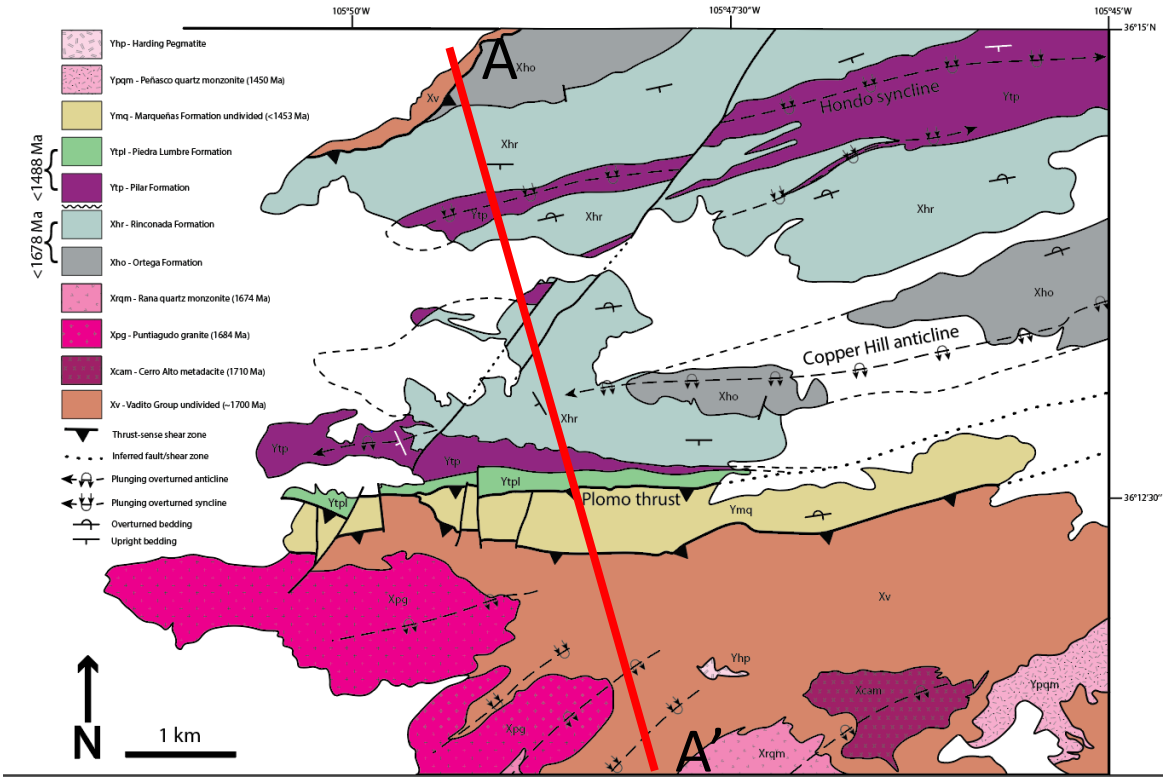

Figure 4: Simplified Precambrian geologic map of the southern Picuris Mountains, NM. Red line is the cross-sectional line of Figure 12. Modified from Bauer et al., in prep.

The contact between the Hondo Group and the Trampas Group is a key contact to look for evidence of what happened between 1.7 Ga volcanism of the Vadito Group, the gradationally related Hondo Group, and the 1.5 Ga basin (presumably marine) sedimentation of the Trampas Group. This contact is well exposed in the Picuris Mountains and in the Rio Mora area. New mapping, structural analyses, and cross sections across this contact have been undertaken in these two ranges.

Picuris Mountains- local stratigraphic comparison of the basal sediments of the Trampas Group

Field descriptions and thin sections of basal chert and schists

The Copper Hill anticlinorium, one of the major F2 structures in the Picuris Mountains, is an overturned anticlinorium characterized by two south-dipping limbs with a series of tight to isoclinal folds making up a broad anticlinal hinge zone (Figure 5A). Structural transposition within these isoclinal folds often obliterates previous sedimentary textures or structural fabric and re-orients the foliation into parallelism with the S2 axial planar cleavage. However, parts of the hinge structure in the Copper Hill anticline are much less transposed by F2 folding and preserve earlier fabrics and stratigraphic relationships between the Hondo and Trampas groups. In one of these broader, less transposed hinge areas (Figure 4) the contact between the Rinconada Formation of the Hondo Group and the Pilar Formation of the Trampas Group is exposed at multiple locations, offering an opportunity to investigate the nature of the contact.

Figure 5A shows outcrop photos and measured sections of the contact zone lithologies. The most distinctive lithology at this contact is a blue-grey garnet-bearing chert that varies from 0.3 to 2 meters thick. It is entirely quartz with no sedimentary structures, even bedding. This lithology occurs just above a sharp contact with the Rinconada Formation. Above this is a varying succession of recessive garnet-bearing

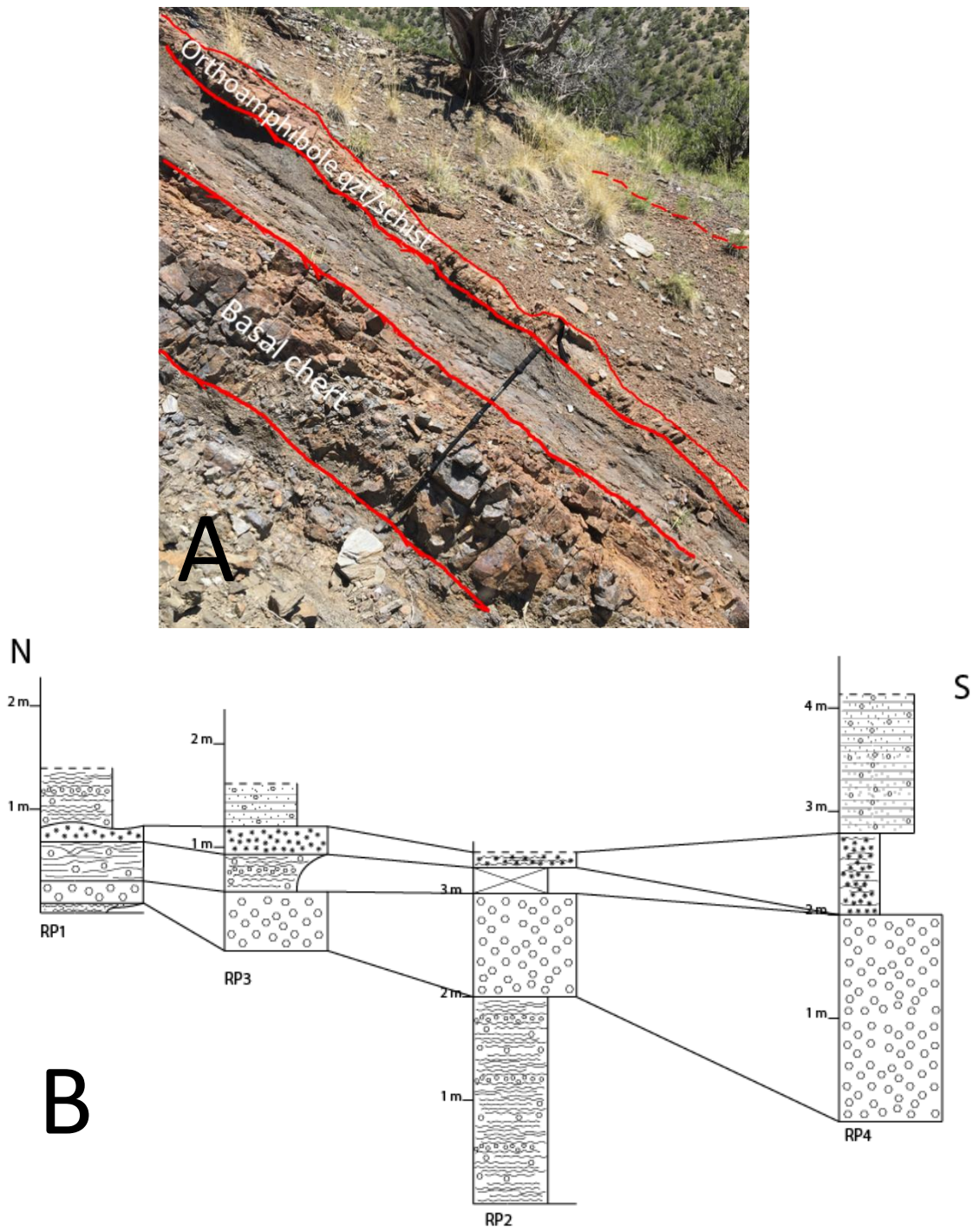

Figure 5: A) Field example of the Hondo-Trampas group contact. In the foreground is the basal chert. Distant from the camera is an apparent gradational transition into Pilar Formation phyllite. Trekking pole is extended to ~1 meter for scale. B) Stratigraphic columns of 4 different outcrops of the Hondo-Trampas group contact found in the hinge region of the Copper Hill anticline. A correlation between outcrops is made based on similar lithology and approximate N-S location.

schists and quartzites, with one distinctive orthoamphibole-bearing schist layer that is

evident in each outcrop examined. The mineralogy of these rocks, individually and collectively, suggest that they could be remnants of a regolith zone that existed during a period of erosion into the underlying Rinconada Formation. The chert is interpreted as a potential paleosol and the orthoamphibole schist as a regolith depleted in Ca relative to Na as is typical of weathered units. The total thickness of this package of contact rocks varies from 1.3-4.2 meters.

Figure 5B correlates four different measured stratigraphic columns from the Hondo-Trampas Group contact where it was found well-exposed and relatively undeformed in the Copper Hill anticlinorium (locations in Figure 4). These columns record a thickening of contact lithology from 1.3 to 4.2 meters from north to south. The basal blue-grey chert mirrors this trend thickening from 0.3 to 2.0 meters from north to south. Other units include a decimeter-thick quartzite that thickens from north to south and schist horizon marked by the presence of orthoamphibole found in both schists and chert. The varying lithology and thickness along the contact within the relatively undeformed hinge zone is compatible with the interpretation that this contact was an erosive surface for some period of time before deposition of the Trampas Group.

Picuris Mountains- structural comparison of fabrics in the Hondo and Trampas Group

Field observations of an early F1 fold generation in the Hondo Group

The hinge region of the major F2 Copper Hill anticlinorium within the Picuris Mountains shows less fabric transposition and provides the area best suited to examine and compare different deformational features and fabrics across the basal Trampas Group

contact (Figure 6). In particular, an area of the hinge region where bedding dips shallowly west was selected for detailed structural analysis.

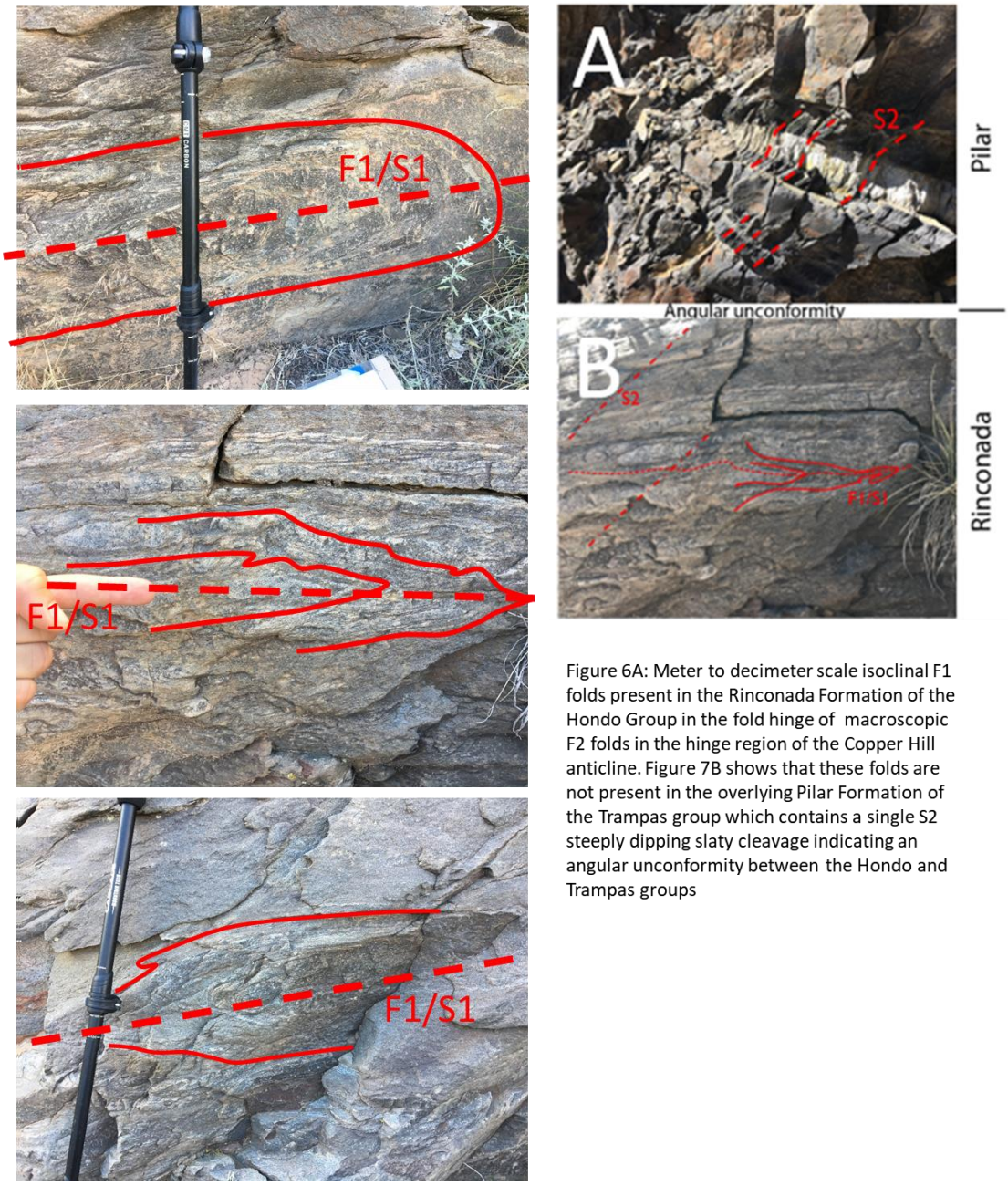

Figure 6A: Meter to decimeter scale isoclinal F1 folds present in the Rinconada Formation of the Hondo Group in the fold hinge of macroscopic F2 folds in the hinge region of the Copper Hill anticline. Figure 7B shows that these folds are not present in the overlying Pilar Formation of the Trampas group which contains a single S2 steeply dipping slaty cleavage indicating an angular unconformity between the Hondo and Trampas groups

Below the contact (Figure 6) there are examples of a generation of F1 rootless isoclinal folds found in the Rinconada Formation at outcrop scale that fold bedding and have an S1 axial plane schistosity. Both style and orientation of these folds differs from

F2 structures and their position in the hinge region indicates overprinting of a bedding-parallel S1 fabric and associated F1 subrecumbant folds by the F2 more upright shortening structures. Asymmetry (vergence) of F1 structures is unclear as they are often symmetric or show both asymmetries in outcrop. The limbs of the folds seamlessly continue into the observed bedding at each outcrop. The examples in figure 6 were found about 20 meters stratigraphically below the Trampas Group contact below and the moderately SW-dipping axial planes are subparallel to bedding in the overlying Pilar Formation that is cross cut by a single steeply dipping slatey cleavage (Figure 6B) and no F1 structures. The Rinconada Schist is a garnet mica schist with a potential turbidite protolith such that soft-sediment deformation structures could possibly explain the folds, but not the S1 cleavage. Thin sections from the limbs of these folds were taken for further analysis of microstructural evidence of the isoclinal fold generation. These results are discussed in more detail below.

Further field work was done to search for evidence of this generation of folds in the Ortega Formation that underlies the Rinconada Formation. No obvious isoclinal folding was found within the sparse oxide-lined sedimentary structures of the quartzite. However, numerous authors have reported a layer-parallel S1 schistosity in the Picuris (Holcombe and Callendar, 1982; Nielson and Scott, 1979; Bauer, 1993) and Tusas Mountains (Kopera, 2003). The possibility of early recumbent folding in the Ortega is not ruled out, but extensive mapping suggests that the early fabric may be related to thrusting (Williams, 1991).

Stereonet analysis

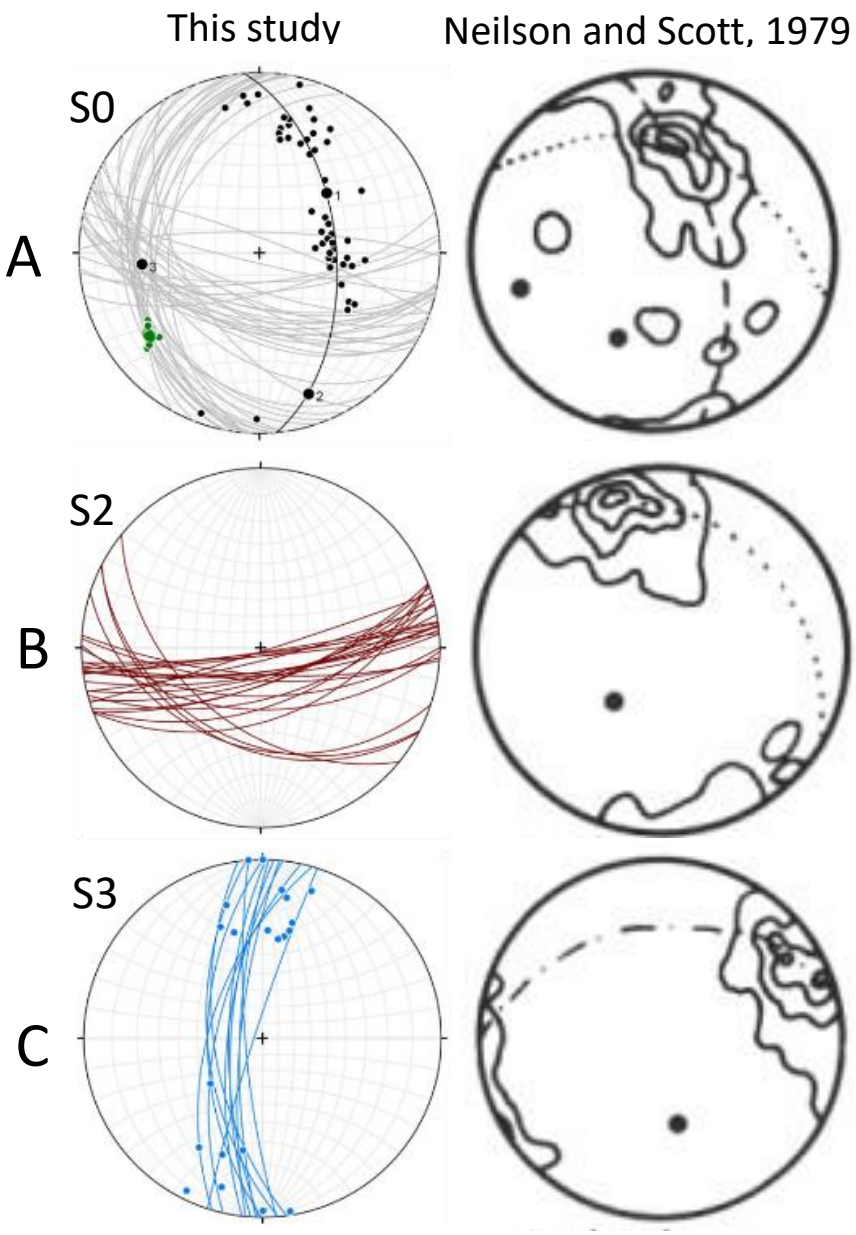

Figure 7: A) Left: stereogram of Pilar S0 bedding planes (grey) and their poles (black), with a cylindrical fit plane run through the poles (n=51). The pole of this cylindrical fit represents calculated fold axis F2 plunging at 35/265. Mean observed minor F2 fold axes is in green at 25/352 (n=8). Right: contoured stereogram of poles to Pilar S0 bedding planes from Nielson and Scott (1979) (n=165). The dashed girdle and associated pole is within ~5° of our girdle and calculated F2. B) Left: stereogram of Pilar S2 axial planar slaty cleavage planes, striking from 069-130 and dipping from 88-47 degrees south (n=26). Right: contoured stereogram of poles to S2 from Nielson and Scott (1979) (n=147). C) Left: stereogram of S3 crenulation cleavage planes and of L3 crenulation lineations (n=12). Right: poles to S3 from Nielson and Scott, 1979.

To further characterize rocks above and below the Hondo-Trampas contact, bedding plane orientations were compared between the Pilar and Rinconada formations within the low-strain hinge zone of the Copper Hill anticlinorium. Seventy-seven S0 bedding plane orientations were measured in the F2 fold hinge region in the Pilar Formation. Figure 7A shows the orientation of the F2 fold hinge (plunging 35 to 265) as calculated from a Pilar S0 pi diagram and the mean of measured S0-S1 intersection and minor fold axis lineations (plunging 25 to 352). The difference between the calculated fold axis (35/265) and the observed minor fold axes (25/233) may be due to a sampling bias more poles from S-dipping limbs than N-dipping limbs. Figure 7B shows S2 slaty cleavage in the Pilar Formation with a mean S2 plane of 081, 64 S. We interpret this cleavage to be axial planar with F2 folds that affect both units.

Figure 7C shows a third generation of folding, S3 crenulation cleavage and L3 intersection lineations that are present in both the Pilar and Rinconada formations. These cleavages strike N-S consistently. Their intersection lineations with S0/S2/S3 surfaces in the Pilar and Rinconada formations are distributed across the great circles of the S3

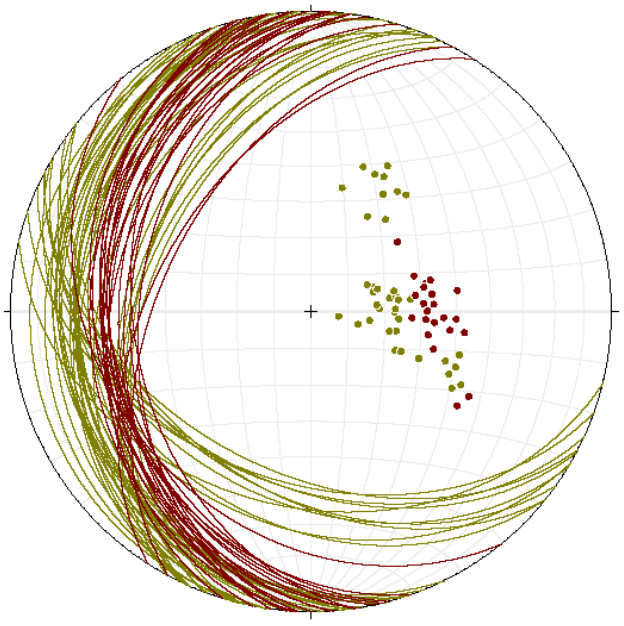

Figure 8: Stereonet of Pilar formation S0 bedding planes compared to Rinconada Formation S0 bedding planes taken from the same F2 fold hinge. Note the variable orientation in the Rinconada bedding planes, and the low angle difference between the cluster of Pilar S0 planes compared to Rinconada S0 planes. N=77

cleavage. This is due to the S0 surfaces being folded by F2 folding. These observed fabrics generally agree with those reported by Nielsen and Scott, 1979 except they inferred more fold generations based on diverse orientations of L3.

Figure 8 shows measurements of Rinconada S0/S1 primary lithological layering plotted with S0 bedding of the Pilar Formation from the same area in the fold hinge of the Copper Hill anticlinorium. The Rinconada S0/S1 planes are more scattered (including more shallow dipping S0/S1 planes and consequently the calculated F2 fold axis plunges ~10 degrees more shallowly than that of the Pilar Formation. This is subtle but would be expected as the underlying Rinconada Formation contains a subrecumbant F1 fold generation and hence more diverse S0/S1 orientations.

Microstructural analysis

Samples for microstructural fabric analysis in the Rinconada Formation were collected near the F2 hinge zone and on an overturned limb of the Copper Hill anticline. All have distinct lithologic layering (bedding), syn-tectonic porphyroblasts of garnet, and multiple penetrative structural fabrics. Figure 9 shows the character of S1 in thin section - a penetrative foliation defined by aligned mica and elliptical quartz grains. This is a metamorphic (not soft-sediment) fabric.

Figure 10 (K92-68) records less strain than Figure 9 (DY17-PL-2), but both contain both S2 and S3. Figures 9 and 10 are annotated for structural fabrics and mineral alignment. K92-68 is cut perpendicular to the strike of primary lithological layering. The composite S0/S1 foliation manifests itself as compositional banding (quartz- and mica-rich domains), as outlined with black lines, and has an orientation of 278/41S, hence is on the limb of an F2 fold. This is interpreted to be a tectonic fabric, not bedding, as shown

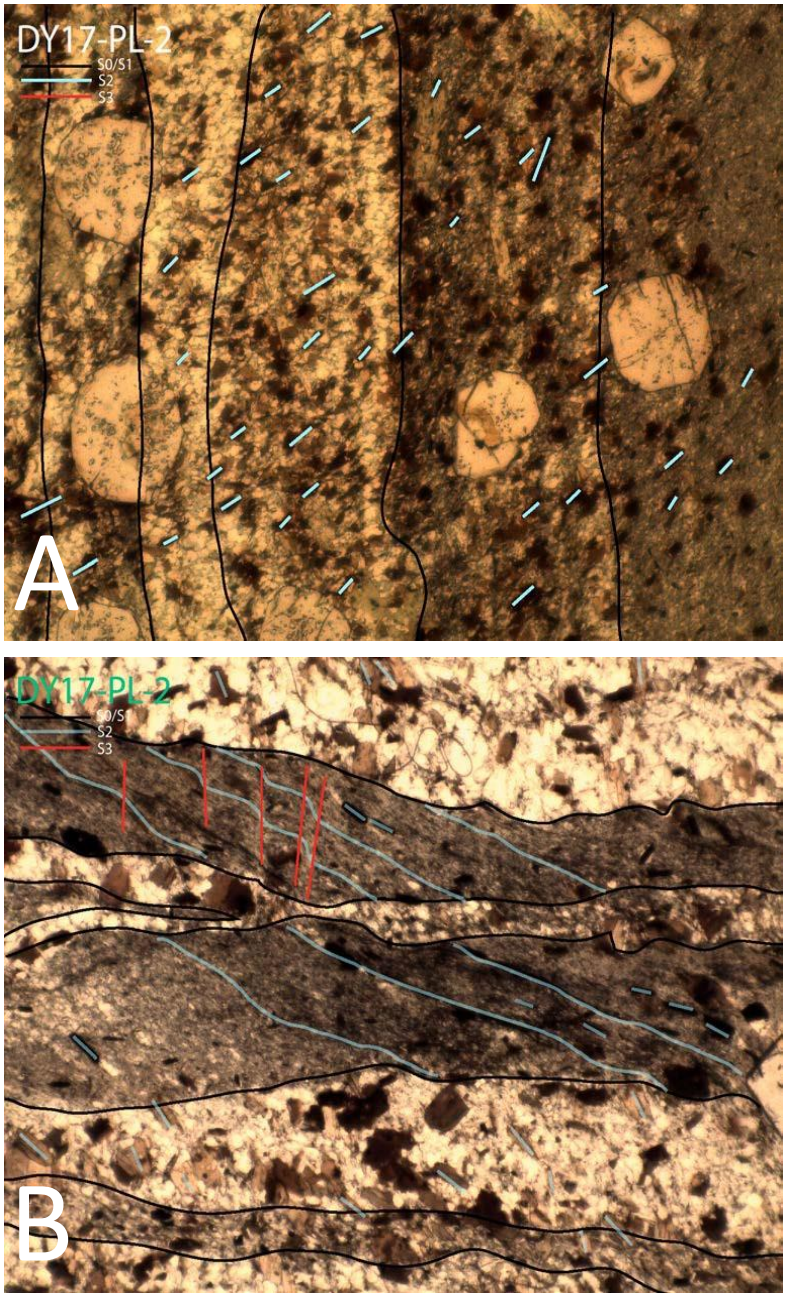

Figure 9: Photomicrographs of section DY17-PL-2 annotated for multiple structural fabrics. S0/S1 is black, S2 is blue, and S3 is red.

by the regular spacing of Q and M domains that resemble a stage 5 differentiated crenulation cleavage (Bell and Rubenach, 1990). S2 is a micaceous schistose cleavage that can be seen strongly overprinting S0/S1 at a ~45 degree angle, defined by the shape preferred orientation of quartz grains and alignment of micas. Biotite porphyroblasts

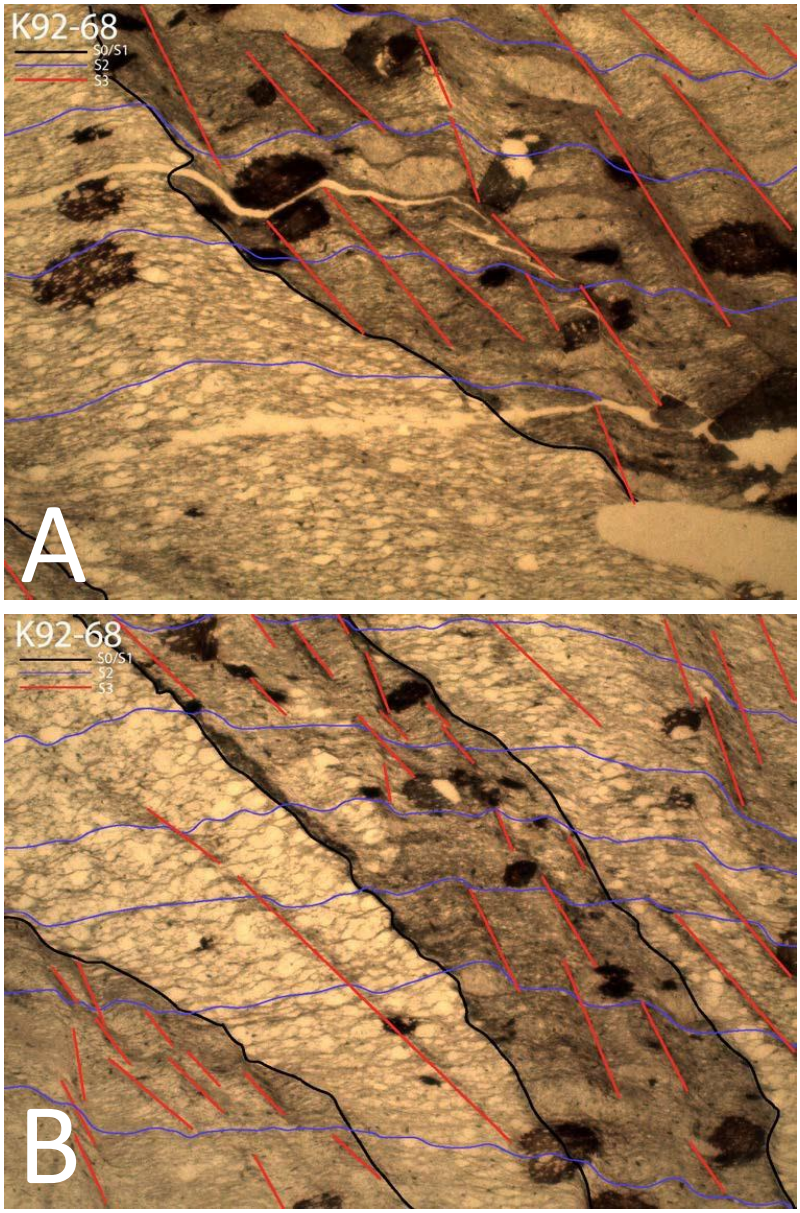

Figure 10: Photomicrographs of section K92-68 annotated for multiple structural fabrics. S0/S1 is black, S2 is blue, and S3 is red.

overgrow S2 with their long axes aligned with S2. S3 is defined by a stage 2 crenulation cleavage mica domains associated with crenulation cleavage and is most easily visible in the micaceous S0/S1 lithological beds. It intersects S0/S1 at a low angle and S2 at a ~60 degree angle. As photomicrograph A in Figure 10 shows, in some areas S3 reaches stage 2 or 3 development of differentiated crenulation cleavage (cf. Bell and Rubenach, 1990).

Figure 9 (sample DY17-PL-2) is from the fold hinge area, and records less D2 strain. Garnets overgrew the unfolded S0/S1 foliation before or early during S2 development supporting a tectonic nature for S1. S2 is more dominant in micaceous layers but less clear than in K92-68, with biotites and oxides aligned along the S2 fabric. In this rock S2 has a similar orientation relative to S0/S1 to K92-68, with S2 intersecting at about 45 degrees to S1. S3 is less well developed than in K92-68. The photomicrograph in figure 9B shows a weak S3 crenulation defined in a S0/S1 micaceous layer intersecting S0/S1 at a high angle to S0/S1. This is distinctly different than the shallow S3 orientation relative to S0/S1 observed in K92-68.

Synthesis of the Hondo-Trampas Group contact

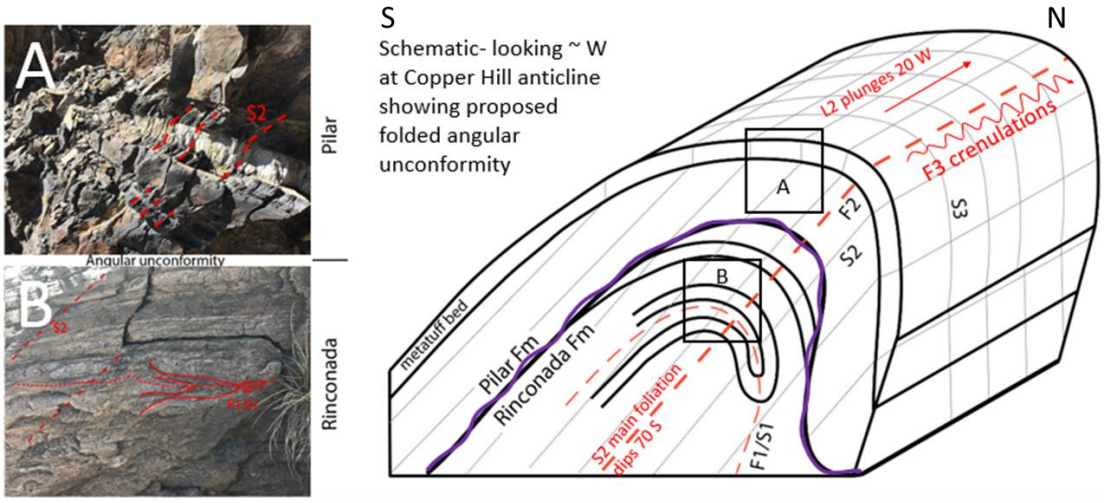

Figure 11: A-B) Structural fabrics observed in the Pilar and Rinconada formations in the hinge zone of the Copper Hill anticline in the Picuris Mountains **A)** S2 slaty cleavage exposed in an outcrop of shallowly dipping Pilar phyllite with interbedded metatuffs. Note the refraction of S2 by the metatuff bed. **B)** An outcrop of Rinconada schist with bedding folded by F1, forming an S1 fabric that defines primary lithological layering. Oblique cleavage S2 can be observed in the less competent layers. **C)** A SW-facing schematic block diagram of observed and interpreted structural relationships in the Pilar and Rinconada. The Rinconada contains F1 folds that are not observed in the Pilar formation. Their contact is interpreted to be a low-angle angular unconformity.

As shown in Figure 11, our synthesis of the observations reported above is that the Hondo-Trampas Group contact is a folded angular unconformity. This contact relationship is only seen in low F2 strain hinges, as all fabrics on the limbs of tight F2

folds are transposed into a composite S0/S1/S2 foliation. The time gaps between Rinconada deposition, D1 deformation, D2 deformation and D3 deformation are unknown. Likewise, the metamorphic grade and P-T-t path difference, if any, between Rinconada and Trampas group rocks is unknown. Future work might investigate additional garnet core or monazite inclusion work, but work so far has been extensive enough to suggest that the D1 parts of the P-T-t path have been so strongly overprinted by peak D2 metamorphism (Daniel et al., 2013) that determining metamorphic grade for D1 will be difficult. Hence, it is possible either that D1 may have formed much earlier (e.g. ~ 1.65 Ga Mazatzal Orogeny) or progressively during ~ 1.5 Ga early Picuris progressive deformation.

Picuris map and cross-section

Figure 12 shows a N-S cross-section of the southern Picuris Mountains with the mild Phanerozoic faulting restored. The numbered areas indicate key geochronologic constraints on sedimentation, metamorphism, and plutonism (Jones et al., 2011; Daniel et al., 2013; Aronoff et al., 2016). Schematically shown is the approximate thrust burial needed to explain observed triple point amphibolite grade metamorphism. Constraints on the modern geometry in the Picuris Mountains are shown along Earth's surface (white band) in the center of the cross section.

Our interpretation of thrust-sense shear zones and thrust sheets in Figure 12, from north to south, is as follows. The northernmost thrust sheet, bounded to the south by the Pilar shear zone, contains polydeformed Glenwoody Formation of the Vadito Group. Only a small section of this thrust sheet is exposed in the northern Picuris Mountains. The Hondo synclinorium/Copper Hill anticlinorium thrust sheet contains penetrative F2

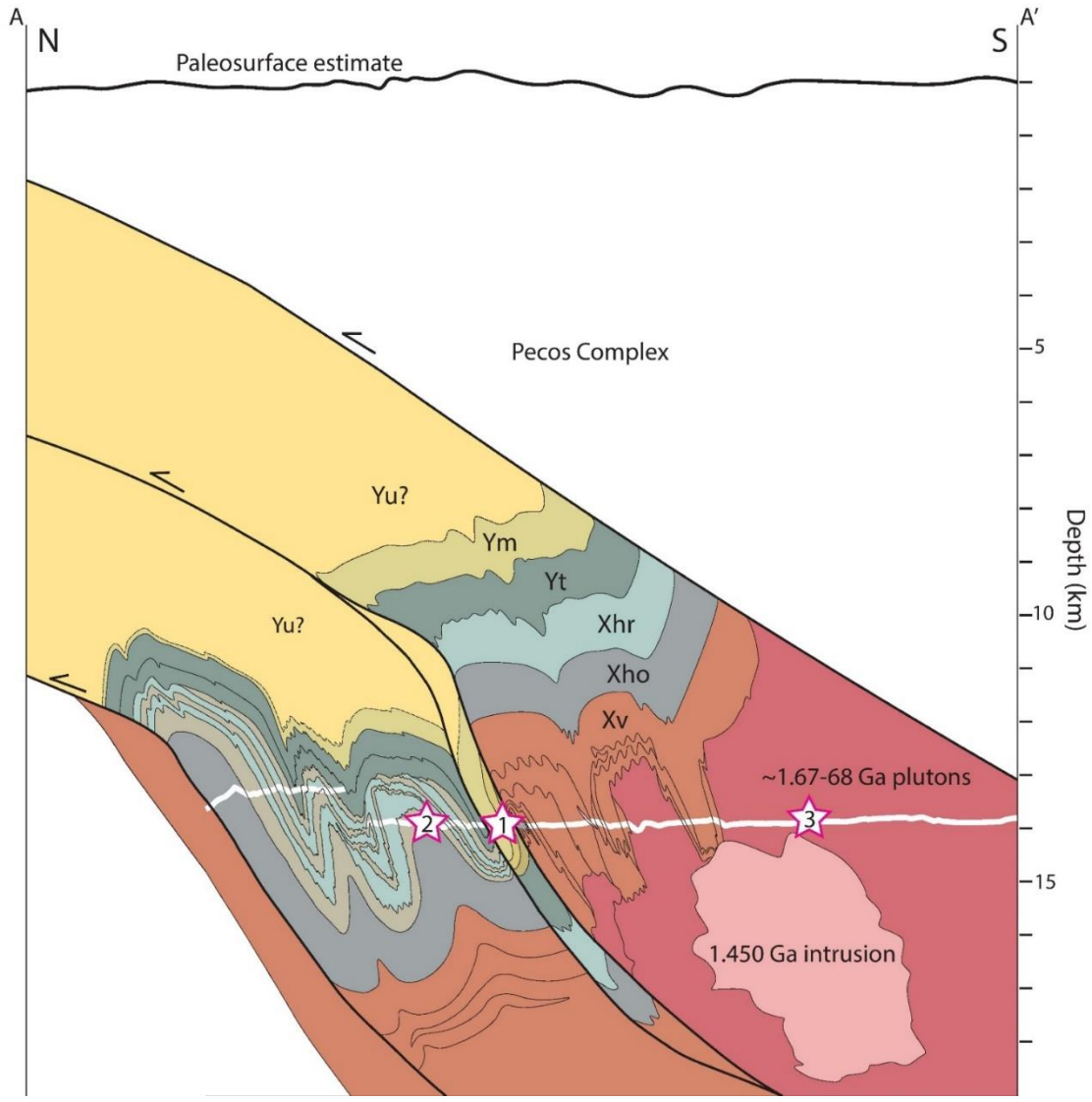

Figure 12: Cross-section of the southern Picuris Mountains with Phanerozoic faulting restored showing the approximate depth of thrust burial needed to explain triple point metamorphism of about 4 kbars. Stars indicate geochronologic constraints as follows: 1) deposition of the Marqueñas Formation at <1453-1450 Ma based on U-Pb dated detrital zircon (Jones et al., 2011); 2) peak metamorphism of basin sediments following burial to 12-14 km based on Lu-Hf garnet ages of 1456 ±16 and 1450 ±6 Ma (Aronoff et al., 2016); 3) Intrusion of the Peñasco quartz monzonite at 1450 ±10 Ma based on U-Pb zircon crystallization ages (Daniel et al., 2013).

folding and S2 axial planar foliation development in the Hondo and Trampas groups and is bounded to the south by the Plomo shear zone. The Plomo shear zone consists of two different shear zones in the southern Picuris that bound the Marqueñas Formation with its

stretched cobble conglomerate. These cobbles define strain ellipses that Neilson and Scott (1979) showed to be L-S tectonites with a steeply SE- plunging stretching lineation compatible with thrusting. The Peñasco thrust sheet contains the polydeformed Vadito Group and 1.45 Ga Peñasco granite. The Pecos shear zone, which outcrops in the Pecos Wilderness area, is interpreted to either be continuous with the Plomo shear zone (Daniel et al., 2013) or projects somewhere south of the Picuris Mountains. The Pecos thrust sheet contains Pecos greenstone belt and farther south the Dalton Canyon sequence (Metcalf et al., 1990). Note the juxtaposition of disparate 1.45 Ga tectonic elements. 1) is the approximate depositional age of the < 1.45 Ga Marqueñas conglomerate; 2) is the region of triple point metamorphism where rocks were 550-650°C and 4 kbar at 1.45 Ga as shown by ages on metamorphic garnets (Aronoff et al., 2016); 3) is the 1.45 Ga Peñasco granite which intrudes the penetratively deformed 1.7 Ga Vadito Group but is itself only weakly deformed. A challenge in the tectonic synthesis section is to restore this cross-section to a reasonable ~ 1.5 Ga geometry just prior to the Picuris Orogeny.

Geochronologic and thermochronologic constraints on the Picuris orogeny

In an effort to try to improve the resolution on timing of tectonism in the Proterozoic of New Mexico, we applied U-Pb monazite dating and $^{40}Ar/^{39}Ar$ thermochronology for rocks of the Rio Mora area. This area has not been investigated by these methods prior to this study.

In-Situ electron microprobe U/Th-Pb dating of monazite

Monazite is a durable geochronometer that can provide a robust chronology even for complex tectono-thermal histories. Monazite often reveals a multi-stage record of compositionally variable growth domains that are commonly produced during repeated metamorphic/fluid events with orogenesis (Williams et al., 1999; Williams and Jercinovic, 2002). In-situ U/Th-Pb microprobe dating of monazite can provide us with a chronology of discrete monazite growth events of the varying compositional domains of monazite itself and thus add the time dimension to P-T-D (pressure-temperature-deformational) history of metamorphic rocks. Deformation can be linked to monazite ages if grain asymmetry can be linked to fabrics. Monazite geochronology may provide a tool to test whether or not we can "see-through" the effects of the Picuris Orogeny to observe geochronologic evidence of previous tectonism, as well as provide new data on the duration of the Picuris orogeny.

Field mapping in the summer and fall of 2018 brought attention to an L-S aluminosilicate schist found in the basal Ortega Formation near the Vadito-Hondo Group

contact in the Rio Mora area, below the Pecos thrust and on the refolded south limb of the

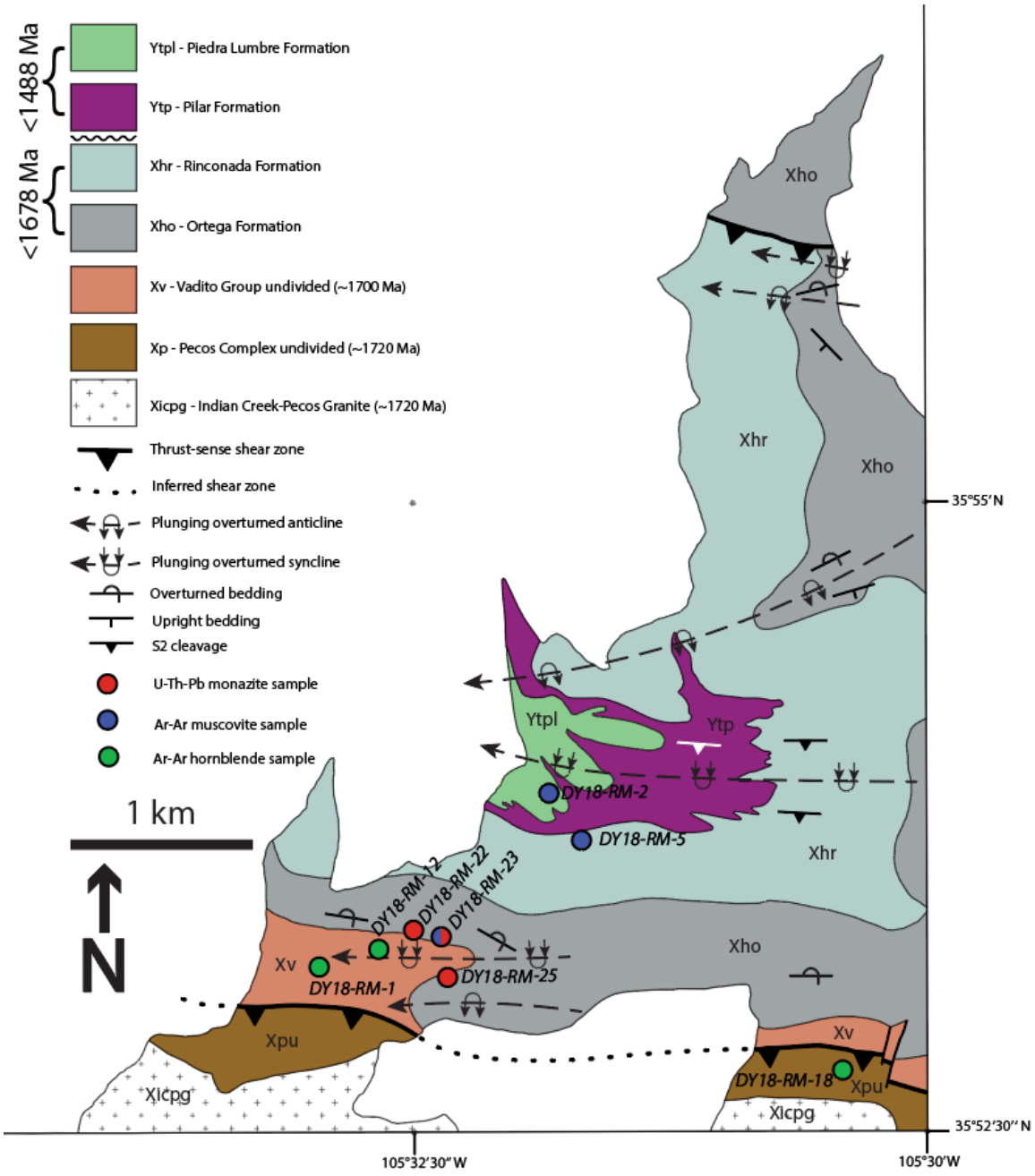

Figure 13: Simplified Precambrian geologic map of the Rio Mora area, NM.

Rio Mora F2 synclinorium (see sample locations in Figure 13). The aluminosilicate schist has a strong E-W to southwest-striking S2 foliation and heterogeneous lineation defined by quartz stretching lineations as well as the orientation of aluminosilicate minerals themselves. The aluminosilicates that define the S2 foliation in this schist vary across a

subhorizontal isograd horizon in the Rio Mora area (Grambling and Williams, 1985). North of this horizon there is abundant sillimanite; to the South, there is kyanite. The orange color of the aluminosilicates (particularly kyanite) in this schist indicate that this horizon is enriched in Mn^{3+} (Gaft et al., 2011). The observation of an Mn-enriched horizon near the Vadito-Hondo Group contact is consistent with previous findings of a regional Mn-enriched horizon in northern New Mexico at the base of the Hondo Group in the Ortega Formation (Grambling and Williams 1985). Being from the ≤1.680 Ga Ortega Formation, these monazite could record domain growth during the Mazatzal Orogeny or any other periods of tectonism bracketed between then and the Picuris Orogeny. Oriented samples DY18-RM-16, DY18-RM-22, DY18-RM-23, and DY18-RM-25 were collected from these outcrops and were slabbed for 30 μm polished thin sections. Microprobe compositional mapping of DY18-RM-16 at the University of New Mexico showed that these rocks contained abundant monazite with multiple compositional domains and would be ideal for in-situ U-Th-Pb dating. Samples DY18-RM-22, DY-18-RM-23, and DY18-RM-25 were chosen for electron microprobe U-Th-Pb monazite dating at the University of Massachusetts Amherst following the methods of Williams et al., 2006 and Williams et al., 2017. Each sample

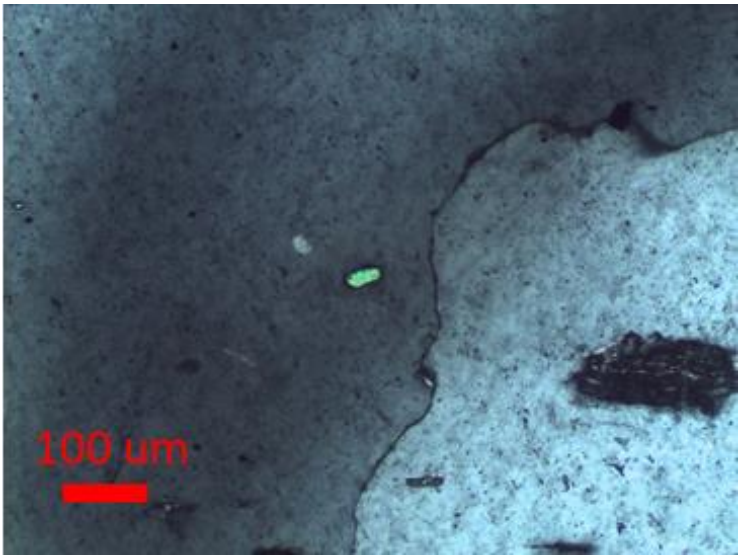

Figure 14: Photomicrograph of monazite target in DY18-RM-23.

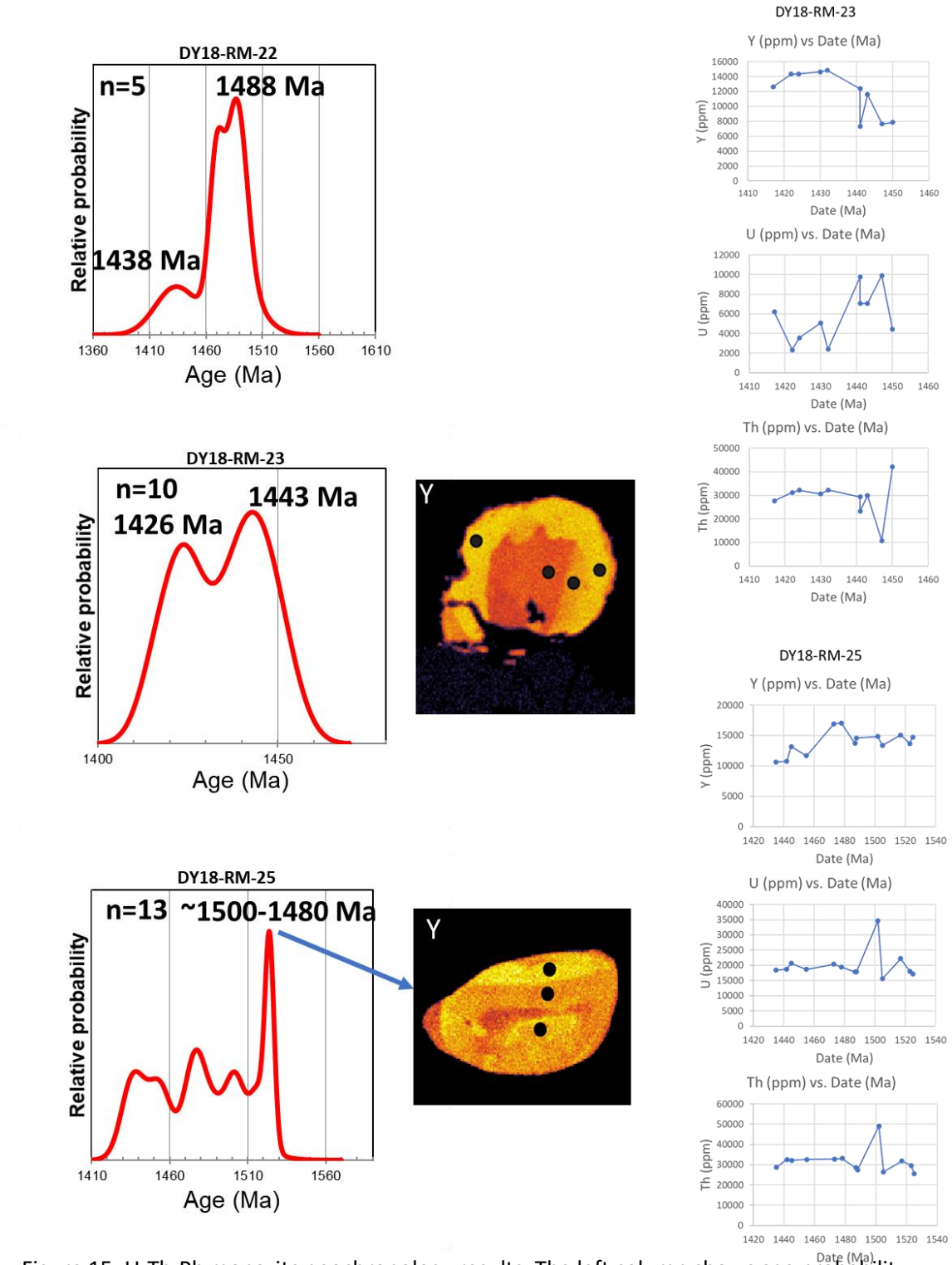

Figure 15: U-Th-Pb monazite geochronology results. The left column shows age probability plots for three Rio Mora samples. Center shows yttrium X-ray concentration maps for representative monazite grains of notable age peaks. The right column shows Y, U, and Th concentrations for monazites in samples DY18-RM-23 and -25. Full analytical data is available in Appendix 1.

were first microstructurally analyzed in a polarized optical microscope, looking for

kinematic indicators and characterizing the aluminosilicate growth in each sample. These thin sections then underwent compositional mapping for Ce and La via electron microprobe at the University of Massachusetts Amherst. The compositional maps were used to identify domains of monazite growth that could be independently dated.

U-Pb-Th monazite dating results

28 U-Pb monazite ages were obtained from monazites from 3 samples from the Rio Mora aluminous unit. Figure 15 shows compositional maps of a representative monazite chosen for dating in each sample. Age probability diagrams from the resultant age analyses for each sample are also shown in Figure 15. Also shown are trace element parts-per million values for yttrium, uranium, and thorium. Individual age analyses can be found in Table 1. DY18-RM-25 shows a prominent peak at ~ 1500 Ma that reflects ages from the center domains identified as cores within monazite grains. An inner core in one grain forms the much smaller peak at 1480 Ma. Outer core ages show another sharp but smaller peak at 1478 Ma. Rim domain ages produce a broad peak from ~1460-1435 Ma with sub-peaks at 1453 Ma and 1438 Ma. DY18-RM-22 produces peaks at 1488 Ma and 1438 Ma, reflecting the core-rim age populations. DY18-RM-23 contains age probability peaks at 1443 and 1423 Ma, though these ages could be affected by high fluid alteration as seen in the affected slightly higher Y domains when compared to samples 22 and 25.

^{40}Ar/^{39}Ar ages from muscovite and hornblende

^{40}Ar/^{39}Ar thermochronology applied to hornblende, muscovite, biotite, and K-spar is useful in assessing both local and regional cooling histories in metamorphic rocks in

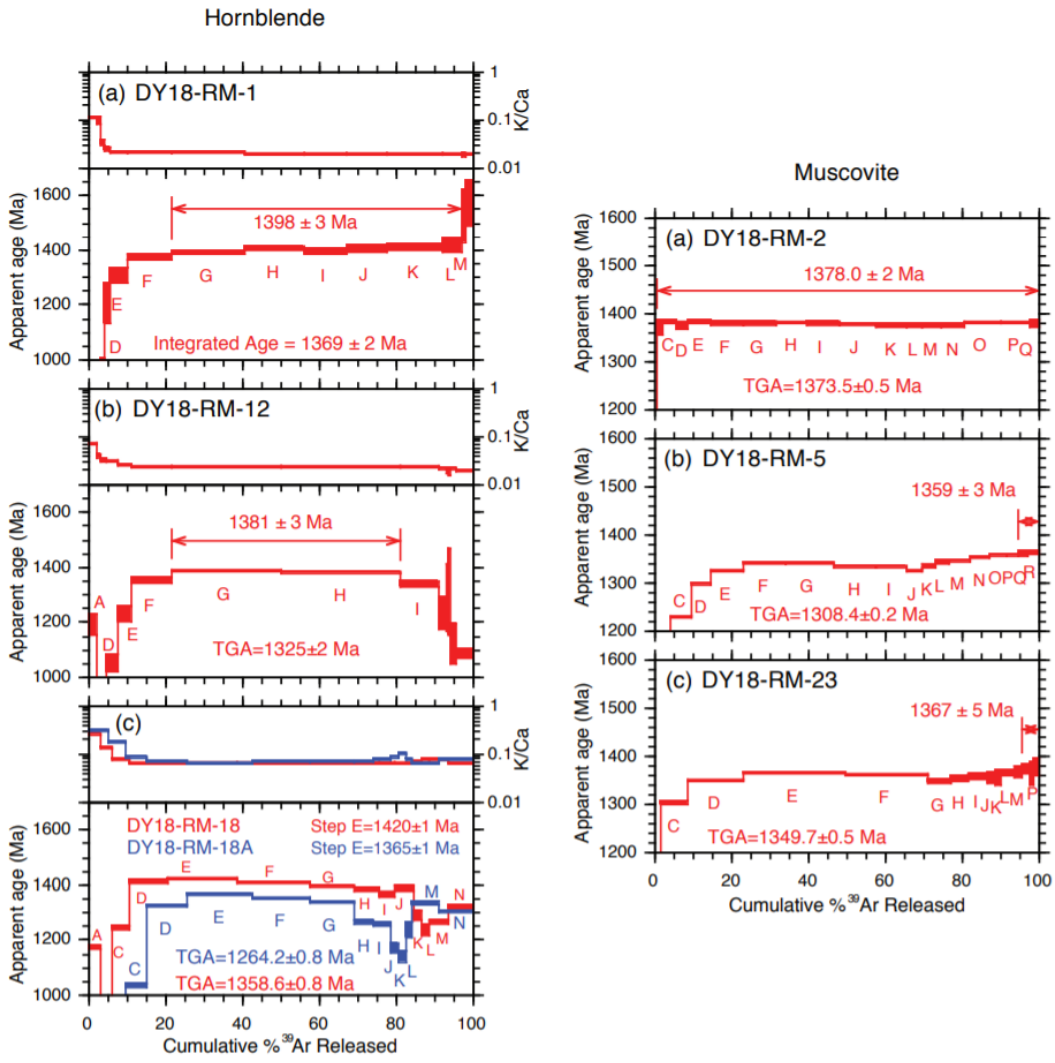

Figure 16: $^{40}Ar/^{39}Ar$ step heating spectra for muscovite and hornblende from Rio Mora. Full analytical data available in Appendix 2.

the range of 500 °C down to 175 °C. Depending in part on cooling rate, hornblende closes to Ar diffusion ~550-500 °C, muscovite ~400-350 °C, and biotite ~350-300 °C. For the purposes of interpretation of new and compiled results in this study, generally accepted closure temperatures for slow cooling through 500 °C for hornblende (Harrison, 1981), 350 °C for muscovite (Harrison et al., 2009) are assumed here. 4 hornblende samples and 3 muscovite samples were collected from Vadito and Hondo Group rocks in the Rio Mora area (see map locations in Figure 13). Sample locations were chosen in the

footwall and hanging wall of the Pecos thrust in an attempt to test for possible temperature gradients that would be evident through different cooling ages found on either side of the thrust. Hornblende sample DY18-RM-1 was sampled from a footwall amphibolite unit in the Vadito Group near contact with the Hondo Group in the southern limb of the defining F2 synclinorium. DY18-RM-18 was taken from an amphibolite interpreted to be either within or in the hanging wall block within the Vadito Group. Muscovite samples DY18-RM-2 and -5 were taken from the Piedra Lumbre and Rinconada formations respectively in the hinge zone of the F2 synclinorium. RM-2 is from a coarser grained muscovite sample with average grain size of 3-5 mm; RM-5 has finer grained muscovite at 0.5-1 mm; sample DY18-RM-23 has coarse muscovite with a range of 5-7 mm taken from a schistose lens from the Mn-rich quartzite at the base of the Ortega Formation south of the F2 syncline.

Figure 16 shows $^{40}Ar/^{39}Ar$ age spectra of the samples. The preferred thermochronologic age on these samples are the selected plateau ages on each of the plotted spectra. Preferred hornblende cooling ages span from about 1398 to 1381 Ma. The single 1420 ±1 Ma step from DY18-RM-18 is an outlier, but overlaps with youngest monazite ages. Muscovite cooling ages span from 1378 ±2 Ma to 1359 ±3 Ma. Coarser grain sizes yield simpler plateaus (DY-2) whereas finer grained muscovites has variable ages at low T steps.

Regional compilation of geochronology and thermochronology

This section discusses our new data in the context of a synthesis of previous geochronology and thermochronology done in the region. Many Precambrian exposures in the central-southern Rockies have been dated using U-Pb and $^{40}Ar/^{39}Ar$ methods in the

past 30 years; our compilation builds on previous compilations from Shaw et al. (2005); Bickford et al. (2015); Aronoff et al. (2016).

Regional compilation of U-Pb igneous zircon dates

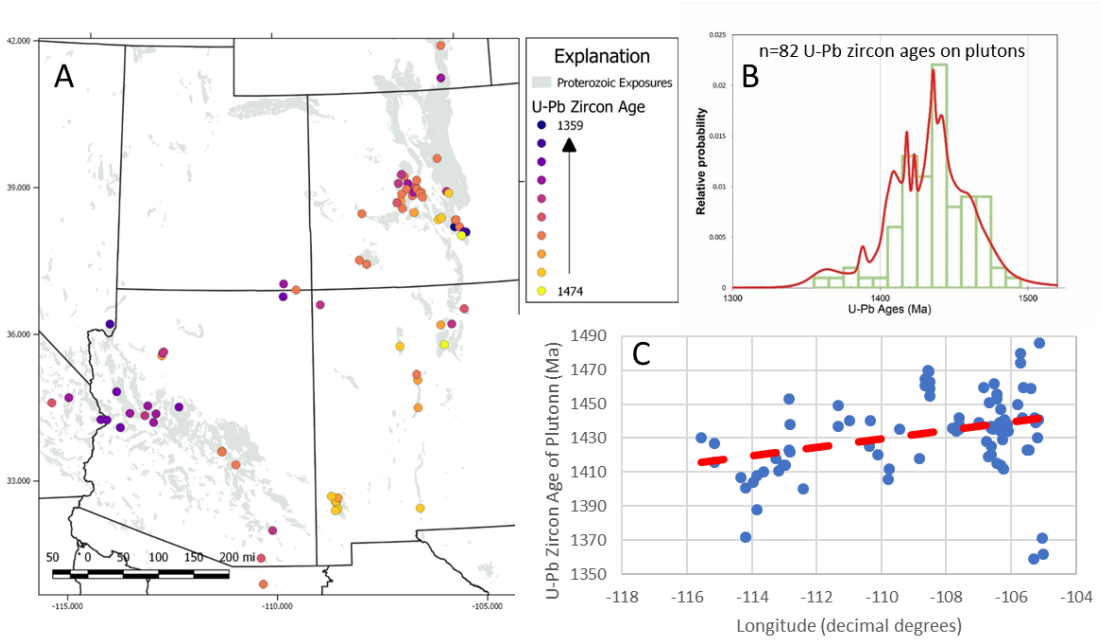

Figure 17: A) Map and B) Histogram and age probability plot of U-Pb zircon ages of Mesoproterozoic plutons in the Southwest. Note an early peak around 1470-1460 Ma, a large peak around 1440, continued magmatism until after 1410-1420 Ma, and latest plutonism 1390-1360 (in the Wet Mountains); n=82 16C. C) Age plotted versus longitude. References are in Appendix 4.

Figure 17 shows the distribution and age probability diagram of compiled U-Pb zircon ages of granitic plutons in the Southwest. Figure 17A shows the distribution of 82 dated granitic plutons in the Southwest compiled from various U-Pb zircon dating work done in the past 40 years. From the histogram, multiple peaks in magmatism between 1.48 and 1.35 Ga can be picked out. Magmatism begins around 1490 Ma and has major activity at 1470 Ma, with a minor dip at 1450 Ma. The most activity can be seen around 1440 Ma, with a peak of over 20 zircons dated to this time frame. Magmatism is then sustained until around 1410 Ma, where a gap in magmatism lasts until 1390 Ma. Then a low peak of ages associated with the southernmost extent of plutons in the Granite-

Rhyolite province lasts from around 1390 to 1360. The oldest age reported is 1486 Ma in the Williams Creek area of the southern Wet Mountains of Colorado, and the youngest age reported is 1333 Ma of the Carrizo-Hackett rhyolite in West Texas, bordering on Grenville-aged tectonism (Bickford et al., 1989; Bickford et al., 2000). Figure 17C shows a subtle younging of plutons from west to east that is complicated by a 50 million year age range between intrusions in many locations. Aside from these few 1.37-1.33 Ga intrusions to the South, these plutons do not seem to show any obvious spatial trends in age. There is no younging direction as might be expected if they reflected changes in dip of a subducting slab.

Lu-Hf ages of garnets

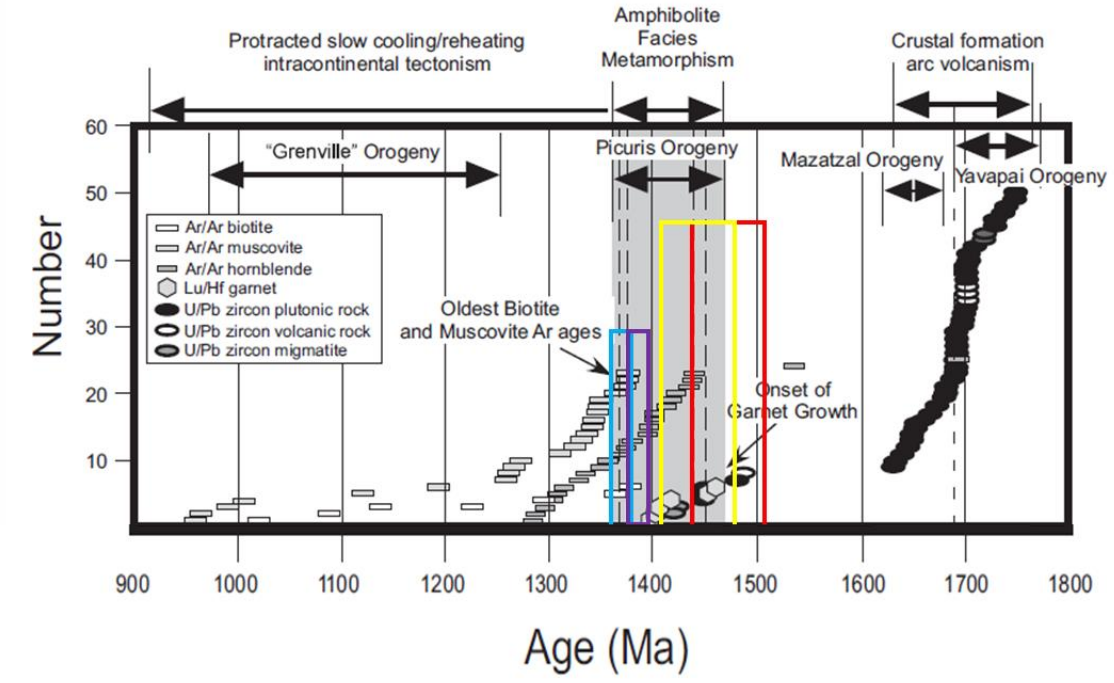

Figure 18: summary ideogram of different metamorphic and plutonic geochronometers. Yellow box shows previously constrained U-Pb/Th monazite ages in Hondo Group exposures near the Picuris and southern Tusas mountains. Red box shows range of new reported monazite ages. Purple and blue boxes show ranges of new hornblende and muscovite $^{40}Ar/^{39}Ar$ thermochronologic ages respectively.

Directly dating metamorphic porphyroblasts such as garnet and staurolite can give insight on timing of both metamorphic conditions and timing of deformation, particularly when fabrics preserved in/overprinted by the porphyroblast can give us information on the exact time of metamorphism relative to deformation. Recent work in the southern Rockies of New Mexico has allowed us to constrain the timing of ~1.4 Ga aged deformation events to a new level of detail. Early work by Lanzirotti and Hanson (1997) and Williams et al. (1999) proposed that the triple point amphibolite facies metamorphism in northern New Mexico took place at 1.4 Ga. This is now confirmed by dating of garnets by Aronoff et al., 2016 who examined the microstructures and fabric relationships of a suite of garnet porphyroblasts whose timing relative to fabric formation ranged from syn- to post-tectonic. Seven garnet ages from this paper range from 1456 ± 16 Ma to 1399 ± 9 Ma, with the oldest age being in the Picuris Mountains and the youngest in the Tusas Mountains (Figure 18). The spread of ages is interpreted to reflect progressive stages of deformation and associated fluctuations in P-T conditions, resulting in multiple periods of garnet growth (Aronoff et al., 2016). This indicates that prograde P-T conditions must have occurred by 1456 Ma. A similar effort to use contact metamorphic minerals around 1.4 Ga plutons in the Manzano Mountains also supported the idea of 1.4 Ga garnet rims grown on older garnet cores (Thompson et al., 1996).

U-Pb-Th monazite ages

Monazite from the southern Rocky Mountains have been dated using U-Pb-Th isotope systems intermittently since the mid-1990's. Monazite dating of Paleoproterozoic quartzites in the Tusas Mountains revealed a younging direction to the South (Kopera, et al., 2002). In the northern Tusas monazite from a series of synclines and anticlines reveal

ages of 1.72-1.7 Ga cores with 1.68-1.65 Ga rims, implying that cores may be detrital but rims may reflect regrowth of monazite during fluid flux associated with the Mazatzal orogeny. In the southern Tusas, monazite show predominantly 1.4 Ga ages from core to rim, indicating that 1.4 Ga tectonism was more pervasive or higher temperature in the

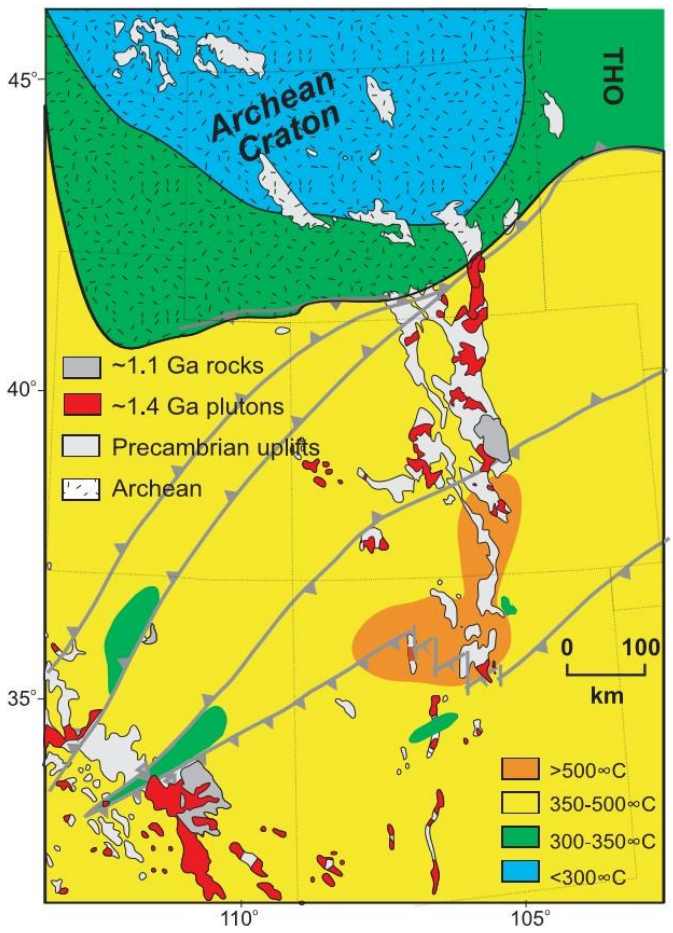

Figure 19: 1.4 Ga regional thermal regimes in the Southwest extrapolated from 40Ar/39Ar closure temperatures of various metamorphic minerals. Note the region around northern New Mexico where temperatures reached greater than 500 °C at about 1.4 Ga (from Shaw et al., 2005).

southern Tusas (Kopera et al., 2002). In the Taos Range and Rincon Range near Taos, monazites dated from similar quartzites range from 1434 Ma-1390 Ma, some of which were contained within aluminosilicates and thus constraining their age to be roughly 1.4 Ga as well (Pedrick et al., 1998; Read et al., 1999). From metamorphic studies, peak

temperature in the Picuris has been estimated at up to 525 °C, with peak pressures being at 4.0-4.2 kbar (Aronoff et al., 2016). No evidence of the Mazatzal orogeny was found in the Picuris monazite (Daniel and Pyle, 2006) although the presence of 1670-1680 granitoids is evidence of Mazatzal age- plutonism. This age of calc-alkaline plutons is also widespread in central and southern New Mexico (Karlstrom et al., 2004). In the Manzano Range to the south, monazite grew during deformation in the aureole of the 1650 Ma Ojito pluton (Karlstrom et al., 2016), refuting interpretations stating that there was no Mazatzal orogeny in the region and emphasizing the importance of understanding spatial variability in the expression of polyphase tectonism.

Regional compilation of $^{40}Ar/^{39}Ar$ muscovite thermochronologic ages

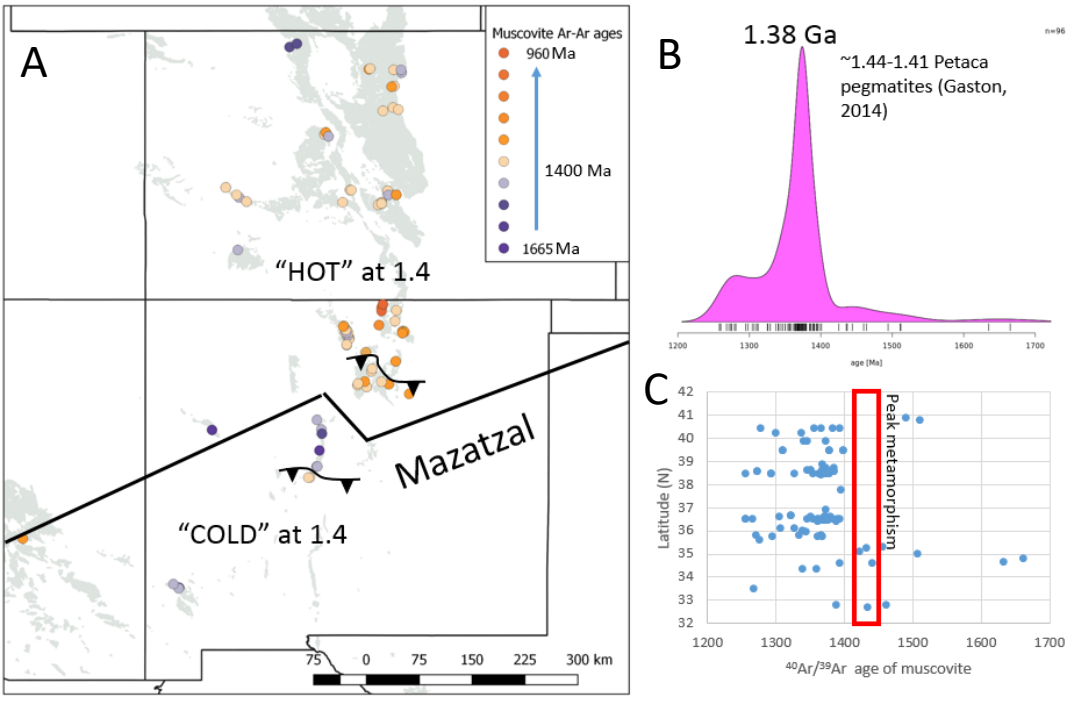

Figure 20: A) Map of compiled muscovite thermochronologic ages (Shaw et al., 2005; Gaston, 2014) including new data. B) Relative age probability diagram of $^{40}Ar/^{39}Ar$ ages of muscovite in northern New Mexico, southern Colorado, and Arizona n=82. C) Muscovite cooling age versus latitude. Note the abundance of cooling well over 100 years past interpreted peak metamorphism. References are in Appendix 3.

$^{40}Ar/^{39}Ar$ ages from hornblende, muscovite, and biotite in central Colorado and northern New Mexico were compiled by Shaw et al. (2005) and are portrayed in Figure 19 as an interpretive " temperature map" of the now-expose middle crustal thermal state of the region at ~ 1.4 Ga. Regions in blue and green preserve old (pre-1.4 Ga) biotite and muscovite ages, respectively, and hence were relatively "cold blocks" and not heated above 300-350 °C during the Picuris orogeny. Regions in yellow have < 1.4 Ga muscovites, but > 1.4 Ga hornblende ages and hence were between 350 and 500 °C at ~1.4 Ga and suggest a regional ambient temperature at 10-15 km depths that would correspond to ~ 30 C/km geothermal gradients with hotter temperatures recorded in the aureoles of 1.4 Ga plutons shown in red. The orange region of southern Colorado and northern New Mexico represents the hottest regions, where hornblendes are 1.4 Ga indicating temperatures greater than 500 °C during the Picuris orogeny.

Additional $^{40}Ar/^{39}Ar$ muscovite thermochronologic ages were run in northern New Mexico by Gaston (2014) in the Picuris and Tusas mountains and are shown in Figure 20. This study concentrated on coarse muscovites from the Petaca pegmatite district that have crystallization ages of about 1430 Ma based on U-Pb/Th dating of monazites from pegmatite samples (Gaston, 2014). The coarse muscovites from these pegmatites have higher closure temperatures of ~400-450 °C and hence can further constrain thermal evolution of the Picuris orogeny. Cooling ages of ~1420 Ma from these coarse muscovites indicates that cooling that lagged tens of Ma following pegmatite emplacement. Figure 20B shows muscovite ages from pegmatites that range from 1.44-1.41 Ga. These are interpreted to be cooling ages rather than crystallization ages and record a tens of Ma lag between pegmatite emplacement and cooling through 400 °C.

Regional cooling ages for finer grained lower closure temperature muscovites shown in Figure 20C gets as young as 1300 Ma.

Discussion of regional timing of deposition and tectonism during the Picuris orogeny

Interpretation of compilation results

Following a 1.6-1.5 Ga lull in magmatic activity known as the "tectonic gap" (e.g. Karlstrom et al., 2004), the Laurentian margin resumed convergent activity. A dramatic marker of this margin today is a belt of A-type plutons and intrusions that stitch different-aged provinces of crust stretching from Southeastern Canada to California (Figure 1). These A-type dominantly granitic (but locally bimodal) plutons intruded heterogeneous Paleoproterozoic crust and extend into the near juvenile younger Granite-Rhyolite province to the south across the Missouri Nd line (Bickford et al., 2015). Individual pluton ages span between 1.48 and 1.35 Ga (Whitmeyer and Karlstrom, 2007; Bickford et al. 2015). A-type magmatism is a common trait of 1.8-1.0 Ga crustal addition to cratons, and past authors have suggested that these plutons are part of a global heating event that happened during the Mesoproterozoic (Haapala and Rämö, 1999; Roberts et al., 2015). In spite of being labeled as "anorogenic" (Anderson and Morrison, 2005), the intrusion of these plutons coincided with significant metamorphism and structural deformation along the modern day southern margin of Laurentia, as will be discussed later on (Kirby and Karlstrom, Nyman et al., 1994; Whitmeyer and Karlstrom, 2007; Daniel et al., 2013).

There is growing evidence that these intrusions were the product of mid-crustal melt generated by heat from mafic underplating and possibly magma-mixing from sources in the lower crust (Frost and Frost, 2010). Lu-Hf isotope data from zircons from these intrusions indicate a range of older crustal sources from the Granite-Rhyolite,

Yavapai, Mojave, and Penokean provinces, independent of each individual intrusion's age but correlative to the crust they intrude. This indicates widespread melting of heterogeneous Paleoproterozoic crust. Mafic underplating following inboard lithosphere delamination has been a proposed heat source for generating this melt (Goodge and Vervoort, 2006; Bickford et al., 2015) as shown by common mafic enclaves in the granites, local bi-modal character (e.g. in the SE Colorado; Gonzales and Karlstrom (1996)), and by petrogenetic models for formation of these "ferroan granites" via mantle-derived mafic parent magmas inducing lower crustal partial melting. Recent work by Marshall et al., 2017 on mantle xenoliths from the Navajo volcanic field indicate that there was a mantle-melt component during this 1.4 Ga event that reset isotopic systems and would support a model for continental backarc magmatism driven by mafic underplating and melting in the lower-middle crust. Previous mantle xenolith and Sm-Nd whole rock dating agrees with this model (Crowley et al., 2006; Bickford et al., 2015).

Age domains in our monazite reflect at least two major stages of growth and diffusion from ~1500 Ma to 1480 Ma and from ~1450-1430 Ma. We interpret these ages to represent peak metamorphic conditions during thrust-induced burial. The first monazite growth event (cores) preceeds or is concurrent with deposition of Trampas Group sediments at <1488 Ma in the Picuris Mountains and is likely the same age as in both Rio Mora and the Pecos. Reconciling this apparent synchroneity between sedimentation and high temperature metamorphism important for understanding the tectonic history of this region and is discussed in the interpretation section. Figure 17 shows that our monazite ages are similar to garnet growth ages and agree with compiles $^{40}Ar/^{39}Ar$ ages of Aronoff et al. (2016) but suggesting onset of the Picuris orogeny

tectonism a bit earlier (~ 1500 Ma) than they show ages and a somewhat longer (~ 140 Ma) duration (1500-1360 Ma).

Restoration of thrusting in the Picuris Mountains from 1.5-1.3 Ga

Existing geochronologic data present a conundrum that products of ~ 1.45 Ga Trampas Group sedimentation, regional peak triple point metamorphism, F2 shortening and granitic plutonism (#1-3 in Figure 12) are all now juxtaposed at the Earth's surface in close spatial proximity in the Picuris Mountain area. Sedimentation of the Trampas

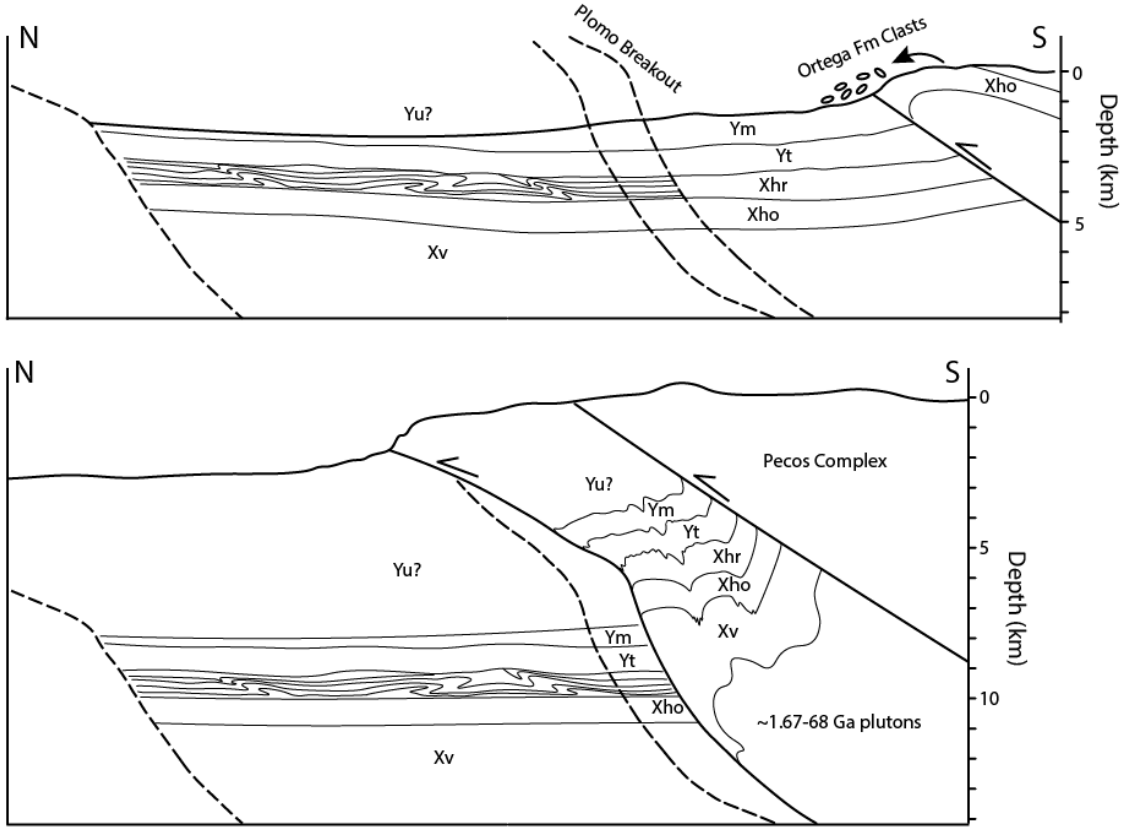

Figure 21: Schematized restorations of the southern Picuris cross section in Figure 12. Top cross section represents ~1453 Ma as the Marquenas formation is being deposited. Bottom section shows the initial stages of thrust stacking to bury the rocks of the Picuris Mountains to the middle crust.

Group had to have been under way by 1488 Ma based on interbedded metatuff U-Pb zircon ages and continued after 1.45 Ga for Marqueñas (Daniel et al., 2013). Aronoff et

al. (2016) found Lu-Hf garnet ages of 1456 ±16 Ma and 1450 ±6 Ma that contained inclusions of an early deformational fabric, and Daniel et al. (2013) determined a U-Pb zircon crystallization age of 1450 ±10 Ma of the nearby Peñasco quartz monzonite. Remarkably, middle crustal metamorphism and magmatism were apparently within error of deposition of the upper Marqueñas Formation at ~1453-1450 Ma (Jones et al., 2011).

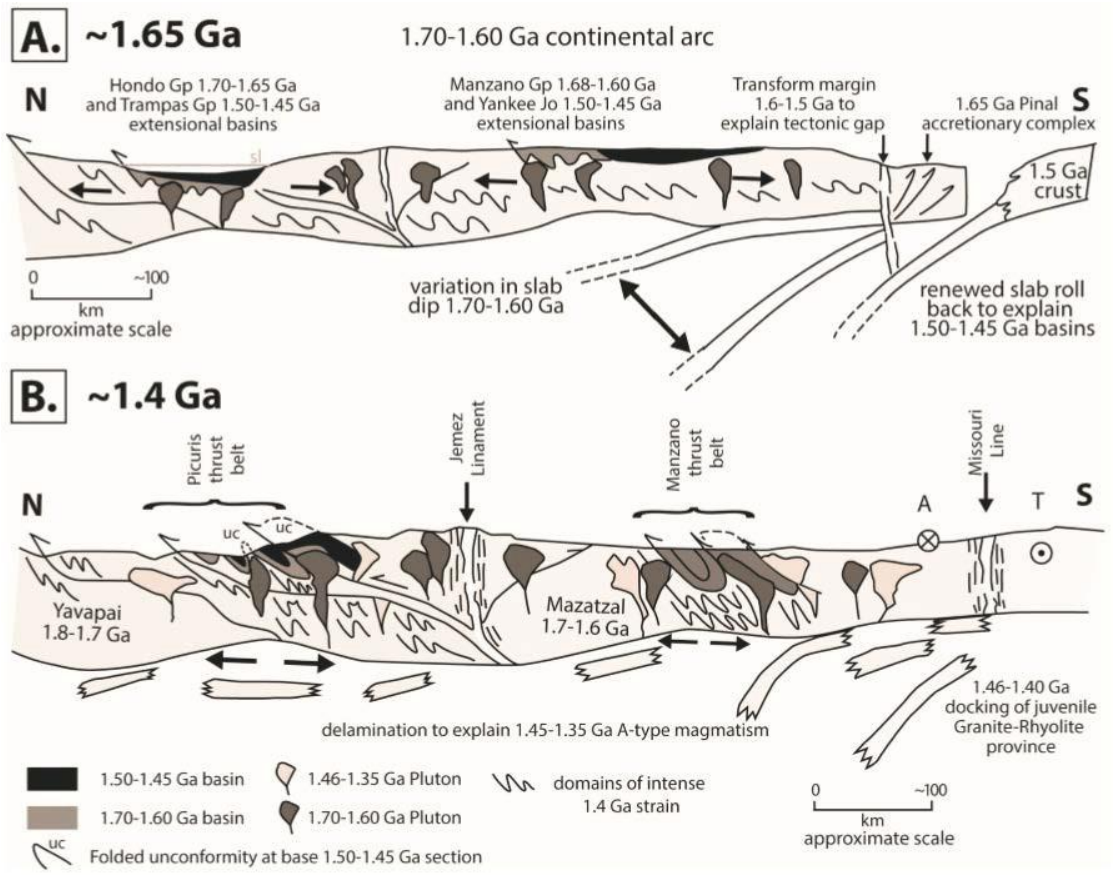

Figure 22: Model for tectonic growth along the southwest margin of Laurentia during the late Paleo and Mesoproterozoic. A) Slab-roll back and backarc extension during the Mazatzal orogeny. A transition to a transform margin around 1.6-1.5 Ga would explain the "tectonic gap" observed in Precambrian exposures along the Laurentian margin. B) The formation of thrust belts around 1.4 Ga to explain observed polyphase deformation, and slab delamination to explain 1.48-1.35 A-type magmatism. Taken from Karlstrom et al., 2016.

Figure 12 shows these relationships in cross-section with the overburden that would be necessary post-thrusting to induce amphibolite-facies metamorphism.

Figure 21 shows schematized restorations of the cross-section in Figure 12 at different stages of progressive thrusting. The earliest stage at ~1453 Ma shows the Trampas/Marqueñas basin during the beginning stages of thrust stacking. In this interpretation, the Marqueñas Formation is a syntectonic package being shed from north-vergent thrusts into a foreland flexural basin. Previous authors agree on a syntectonic depositional environment for the Marqueñas Formation (Jones et al., 2011; Daniel et al., 2013; Aronoff et al., 2016). The second stage shows burial following deposition of the Marqueñas Formation. The burial shown is a product of additional sedimentation and progressive thrust stacking.

Incorporating this with the structural evidence presented in this paper for an angular unconformity between ~1.68 and ~1.48 Ga rock packages, there is reason to believe that the most appropriate model for tectonism during the Paleo- and Mesoproterozoic along the Laurentia margin in the present-day Southwest should incorporate at least two major orogenic events. A recent model proposed by Karlstrom et al. (2015) (Figure 22) proposes an inboard location (not plate collision) location for the Picuris Mountains and intracratonic magmatism for the 1.45 Ga magmatism. This is more compatible with Daniel et al. (2013) alternative B of their Figure 10, not alternatives A which posits inboard 1.49-1.46 extension, C which shows a 1.49-1.46 Ga subduction-related magmatic arc in northern New Mexico, or D, which shows Pilar Group as a 1.49-1.46 Ga passive margin. Figure 22 suggests slab roll back during the Mazatzal Orogeny and later conversion into a transform margin during 1.6-1.5 Ga to explain the observed "tectonic gap" (Karlstrom et al., 2004). The Picuris orogeny would later result in the formation of the Manzano and Picuris thrust belts, and slab delamination and related

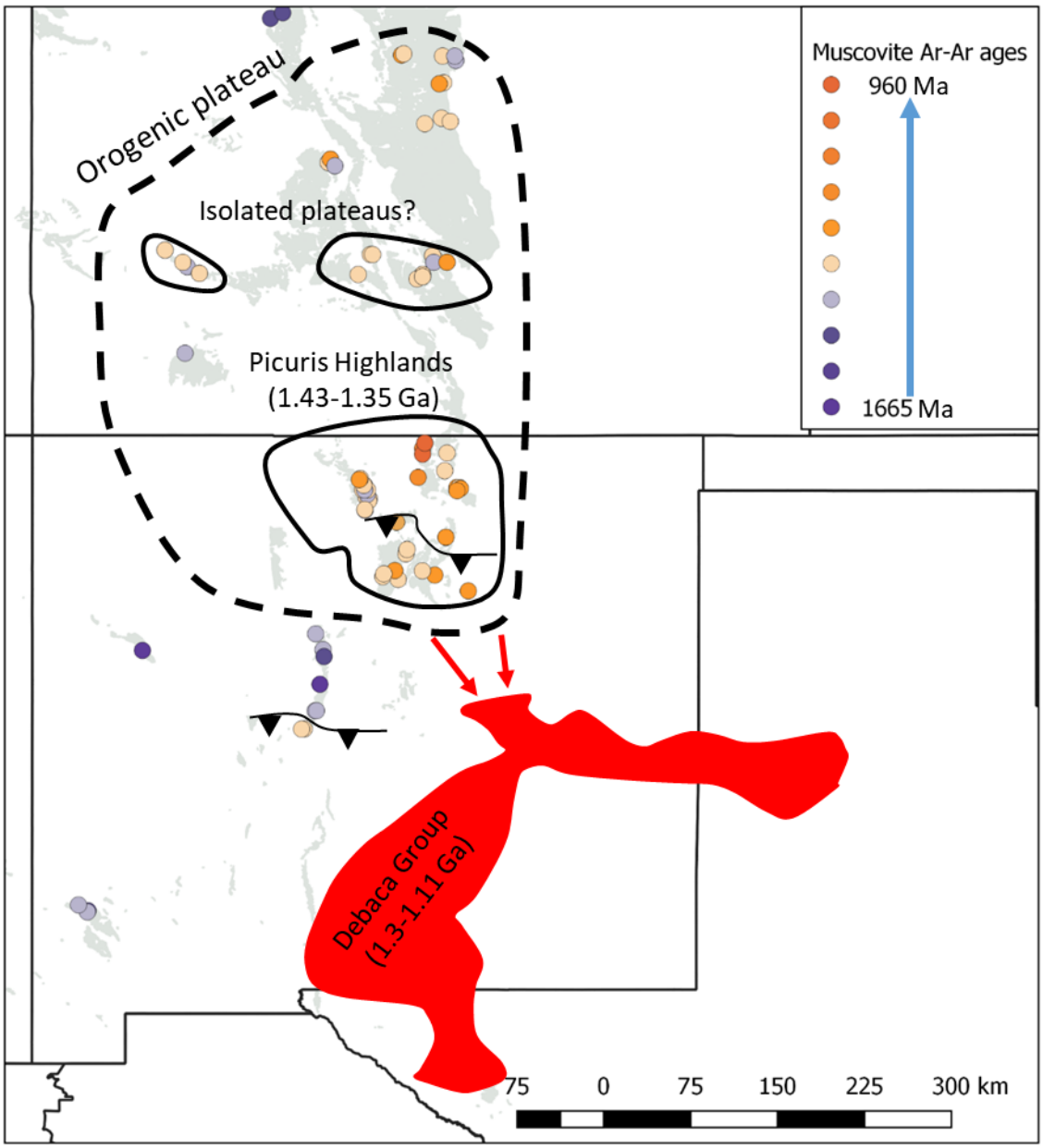

Figure 23: Map of estimated orogenic plateau and other possible areas of uplift based on $^{40}Ar/^{39}Ar$ cooling ages of muscovite. The Debaca Group footprint is shown in red (Amarante, 2001).

mafic underplating would explain the bloom in A-type magmatism from 1.48-1.35 Ga. This model could account for the creation of a folded angular unconformity due to polyphase tectonism as this paper reports, while fitting into the metamorphic and magmatic constraints placed by previous work.

To explain the Ar-Ar data, as well as the intense intracratonic deformation seen in the Picuris orogeny, we also suggest the development of an orogenic plateau or mountain belt. Potential analogs for modern orogenic plateaus include the Colorado Plateau, Altiplano–Puna, or Tibetan plateau (Figure 24). While none of these is likely an exact

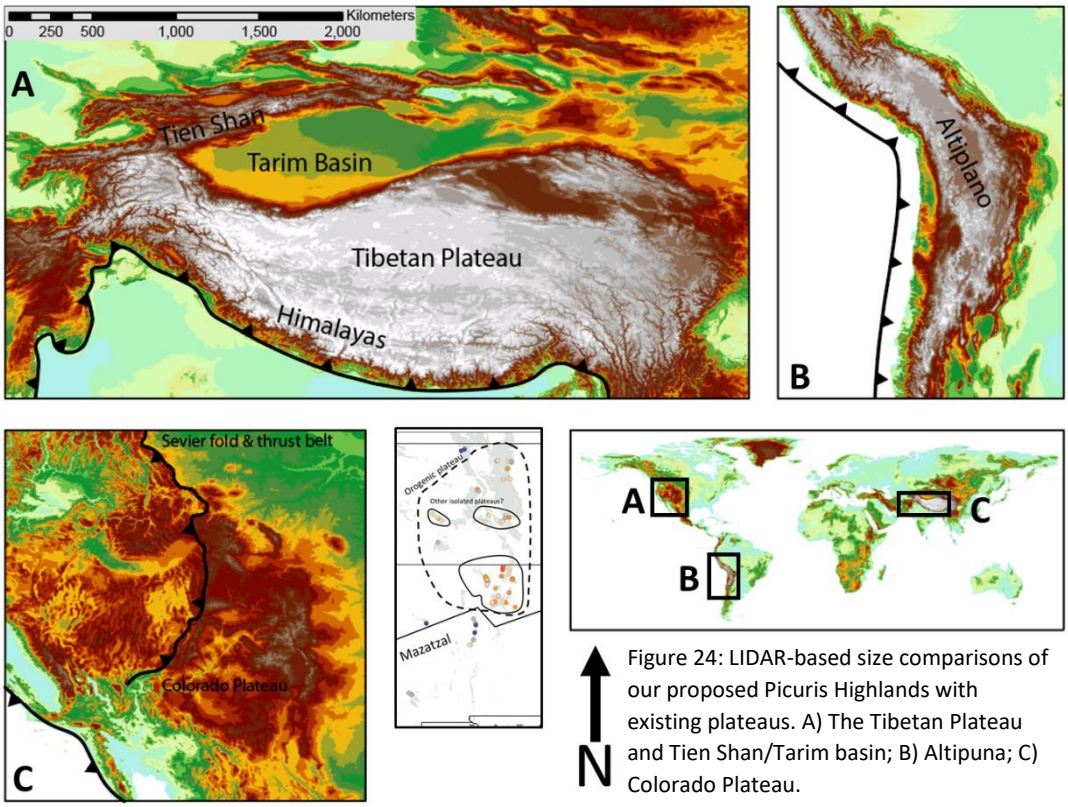

Figure 24: LIDAR-based size comparisons of our proposed Picuris Highlands with existing plateaus. A) The Tibetan Plateau and Tien Shan/Tarim basin; B) Altipuna; C) Colorado Plateau.

analog, aspects of each might help explain the Picuris orogeny and its aftermath. The Colorado Plateau is part of the western US region that was uplifted from sea level at 70 Ma to 2 km elevations at present in several stages due to flat slab subduction at the plate margin 1000 km to the west, slab foundering and asthenospheric return flow in the mid Tertiary, and ongoing differential uplift due to small scale mantle convection. The middle tertiary ignimbrite flare-up part of its uplift history produced similar rhyolitic caldera eruptions likely fed by A-type plutons similar to the 1.45 Ga plutons, both generated by mafic underplating. Middle crustal contractional deformation via channel

flow is possible (McQuarrie and Chase, 2000). Thrust-related flexural basins are present in Laramide syncontractional basins, but the degree of intracratonic penetrative deformation is much less than for the Picuris Orogeny and the only similar deformation might be in the Maria fold and thrust belt, closer to the plate margin.

The Altiplano-Puna plateau is a 3-4 km high plateau that is part of the Andean convergent orogeny above a flat slab segment of the downgoing Nazca plate. The type of caldera-related magmatism may be similar to the delamination magmatism that may also explain the 1.45 Ga granites (Kay and Kay, 1993). The Tien Shan-Tarim Basin region of China is a helpful analog in describing the synchronous sedimentation and tectonism that is interpreted to have happened in the Picuris Orogeny. Late Oligocene-early Miocene shortening in this region involved multistage uplift of the Tibetan Plateau and Parim regions, while the Tarim block was dropped and thrust under the modern Tien Shan region. Continued convergence formed the maximum uplift of the modern Tien Shan (Buslov et al., 2006). During this ~20 million year interval, syntectonic sedimentation occurred within Tarim basin. The >1000 km distance from the plate boundary (figure 24) would also be an accurate comparison to the location of our highlands assuming the plate boundary at the time of the Picuris orogeny was located at the Granite-Rhyolite Province transition (figure 1) (Whitmeyer and Karlstrom, 2007).

Our two main reasons for proposing that the Picuris Orogeny built a high mountain belt or plateau are: 1) the 50-100 Ma (1.48-1.42 Ga) of penetrative thrusting and shortening, and 2) the 50-100 Ma (1.42-1.35 Ga) of slow cooling recorded in the Ar-Ar data between peak metamorphism and the Ar-Ar cooling ages. This slow cooling history would be expected for erosional exhumation of any of the plateaus mentioned

above. The Ar data compilation can also help constrain the boundaries of our proposed elevated plateau in terms of different cooling histories of hot and colder blocks. The resulting interpreted size of the Picuris orogenic plateau is shown in Figure 23. The eastern margin is shown at the present Rocky Mountain front, where 1.45 Ga middle crustal plutons (to the west) are juxtaposed with 1.45 Ga shallow level plutons and rhyolites. The southern margin is drawn to exclude the "cold block" of the Manzano thrust belt although the Sandia granite has a protracted cooling history similar to Picuris area. The northern boundary would likely exclude the Needle Mountains where 1.7 Ga muscovite Ar ages are preserved (Karlstrom et al., 2016). The western boundary is no constrained. As drawn, our proposed plateau is smaller than the overall Tibetan Plateau but similar in size to the Tien Shan. It is slightly smaller than the Colorado Plateau, and similar in size to the Altiplano. The slow erosional removal of this plateau would provide a mechanism to have protracted cooling from >500 to <350 °C after 1410 Ma, lasting to past 1300 Ma. A possible orogenic plateau analog would be the construction and eventual erosional removal of the Colorado Plateau from its initial uplift ~ 90 Ma to its future erosion back to sea level tens of millions of years in the future. In such an analog, erosional removal of a 2 km high Colorado Plateau and progressive 4/5 isostatic rebound would require exhumation of rocks from 10-15 km depths, similar to those found in the aftermath of the Picuris 0rogeny. Erosional demise of the plateau may have provided detritus for deposition of metasedimentary units in the ~ 1.2 Ga Debaca Group. The Debaca Group is a sequence of weakly metamorphosed metasedimentary and metavolcanics intruded by a 1.09 Ga gabbro and overlying a 1.33 Ga quartz syenite, constraining the exact age of the unit between 1.09-1.3 Ga (Amarante, 2001). It is

distributed in the subsurface of southeastern New Mexico, stretching into west Texas and the Texas panhandle region. It has been suggested that this unit is correlative with other weakly metamorphosed ~1.1 Ga sedimentary groups in the southwest such as the Unkar and Apache groups of Arizona (Amarante, 2001).

Conclusions and discussion of the Picuris orogeny

The Picuris orogeny was characterized by 1.50-1.45 Ga syntectonic basins, 1.45-1.43 Ga syntectonic pluton emplacement and peak metamorphism near the aluminum silicate triple point, formation of subvertical cleavage including the main E-W subvertical fabric and shear zones in the Picuris Mountains, and a prolonged 1.45-1.35 Ga cooling history. These aspects are interpreted below.

The generation of F1 isoclinal folds in the found in the upper Hondo Group do not appear to be a result of soft sediment deformation but instead are evidence of a recumbent folding event, likely related to thrusting, that is not recorded in Trampas Group metasediments. A potential regolith along the contact, and more dispersion of bedding plane measurements below versus above the contact are permissive of a low-angle unconformity between the uppermost Hondo Group and lowermost Trampas Group sediments. Such an unconformity may record the end of a long period of erosion from ~1.67 to 1.48 Ga between deposition of the two groups. The age of the F1 structures is unknown as these were strongly overprinted by Picuris Orogeny-associated F2 structures. The duration and penetrative nature of the F2 and F3 contractional deformation, and 4 kbar peak metamorphism lead us to envision a regional scale thrust-related deformation that took place within previously accreted older crust of the Mazatzal province. New U/Th-Pb monazite geochronology in the Rio Mora area helps further constrain both the

onset and duration of the Picuris Orogeny. Aluminosilicate schists/gneisses from the Hondo-Vadito group contact provide monazite with core age populations panning from ~1500-1480 Ma, implying that significant heating and fluid flow were underway synchronously with Trampas Group sedimentation in the Picuris (Daniel et al, 2013). Precipitation rim age populations as young as 1426 Ma indicate that tectonism could have spanned 60 years following initiation, or that there were distinct pulses of monazite growth associated with pulses of tectonism. These ages overlap with previously established dating of deformation in the Picuris and Tusas mountains from 1456 Ma to 1400 Ma (Aronoff et al., 2016).

Compiled U-Pb zircon crystallization ages from exposed 1.48-1.35 Ga plutons in the southwest indicate that while subtle younging directions can be worked out NE-SW, there are no younging relationships N-S that would indicate slab angle fluctuation. The tectonic explanation for the regional bloom of intracratonic 1.45-1.35 Ga A-type magmatism may involve basaltic lower-crustal underplating related to upwelling asthenosphere below a continental margin orogenic plateau, analogous to delamination magmatism associated with the ignimbrite flareup. This is evidenced by the presence of mafic enclaves in many of the exposed Mesoproterozoic plutons.

Compiling new $^{40}Ar/^{39}Ar$ thermochronologic ages of muscovite and hornblende from Rio Mora with previous work on muscovite in southwestern basement exposures provides evidence for slow-cooling from ~1.42-1.3 Ga following the Picuris orogeny in basement exposures in northern New Mexico and south-central Colorado. Peak temperatures at ~1450 Ma would be equivalent to ~550-600 °C. Temperature in the middle crust of northern New Mexico and southern Colorado would have to fall to <350

°C by ~1350 Ma. This would equate to ~2 °C/Ma of cooling (200 °C in 100 Ma). Mapped thermochronologic ages of muscovite also reveal that older ages of muscovite are preserved south of the Yavapai-Mazatzal crustal province boundary, indicating that heating in much of this region did not exceed 350 °C during the Picuris orogeny. We interpret that the region to the north of this boundary extending to central Colorado, east to the edge of the front ranges, and west to at least the San Juan Mountains were part of an orogenic plateau or highlands. Given the ~ 60 Ma (1480-1420 Ma) of penetrative deformation and high-grade metamorphism, we infer the construction of an orogenic highlands comparable in scale to the modern Tien Shan region, far behind the convergent plate margin, but of major plate tectonic proportions. Similarly, the >100 Ma of slow cooling through ~350 °C in muscovite (~1450-1350 Ma) is best explained by the initial stages of the denudation of this orogenic highland.

In summary, to reconcile these new and compiled datasets, we propose the following model for tectonism in northern New Mexico during the Picuris orogeny. Inboard stacking of thrusts initiated during Trampas Group sedimentation around 1490-1480 Ma, creating a syntectonic basin in which conglomeratic units like the Marqueñas Formation were deposited (Figure 21). Thrust stacking continued until the Plomo-Pecos thrust belt was buried sufficiently to induce amphibolite-faces metamorphism from ~1450-1420 Ma and allow for emplacement of plutons. This shortening constructed an orogenic plateau residing over at least northern New Mexico and south-central Colorado that persisted beyond ~1.3 Ga, as suggested by the compiled thermochronologic data in muscovite. The Debaca Group may be a possible product of the gradual erosion of this

plateau. More investigation is needed on the possible lateral extent of slow cooling into southern Arizona and the Great Plains to understand the extent of this orogenic plateau.

References cited

Amarante, J.F.A., 2001, Characteristic of the basement rocks in the Mescalero 1 well, Guadalupe County, New Mexico (MS thesis): Socorro, New Mexico Institute of Mining and Technology, p. 73

Anderson, J.L., Morrison, J, 2005, Illmenite, magnetite, and peraluminous Mesoproterozoic anorogenic granites of Laurentia and Baltica: Lithos, v.80, no.1-4, p.45-60

Aronoff, R. F., Andronicos, C.L., Vervoort, J.D., and Hunter, R.A., 2016, Redefining the metamorphic history of the oldest rocks in the southern Rocky Mountains: GSA Bulletin, v.128, no.7-8, p. 1207-1227, doi: 10.1130/B31455.1

Bauer, P.W., and Williams, M.L., 1989, Stratigraphic nomenclature of Proterozoic rocks, northern New Mexico— Revisions, redefinitions, and formalizations: New Mexico Geology, v. 11, no. 3, p. 45–52

Bauer, P.W., 1993, Proterozoic tectonic evolution of the Picuris Mountains, northern New Mexico: The Journal of Geology, v. 101, p. 483–500, doi:10.1086/648241.

Bauer, P.W., and Helper, M.A., 1994, Geology of Trampas quadrangle, Picuris Mountains, Taos and Arriba counties, New Mexico: New Mexico Bureau of Mines and Mineral Resources Geological map 71, scale 1:24,000, 2 sheets

Bell, D.A., 1985, Structural and age relationships in the Embudo Granites Picuris Mountains, New Mexico (MS Thesis): Dallas, University of Texas at Dallas

Bell, T.H., and Rubenach, M.J., 1990, Crenulation cleavage development—evidence for progressive bulk inhomogeneous shortening from “millipede” microstructures in the Robertson River metamorphics: Tectonophysics, v. 68, i. 1-2, p. T9-T15

Bickford, M.E., Shuster, R.D., and Boardman, S.J., 1989, U-Pb geochronology of the Proterozoic volcano-plutonic terrane in the Gunnison and Salida area, Colorado, in Grambling, J.A., and Tewksbury, B.J., eds., Proterozoic geology of the southern Rocky Mountains: Geological Society of America Special Paper 235, p. 33–48

Bickford, M.E., Soegaard, K., Nielsen, K.C., and McLelland, J.M., 2000, Geology and geochronology of Grenville-age rocks in the Van Horn and Franklin Mountains area, west Texas: Implications for the tectonic evolution of Laurentia during the Grenville: Geological Society of America Bulletin, v. 112, p. 1134–1148, doi: 10.1130/0016-7606(2000)112 <1134:GAGOGA>2.3.CO;2

Bickford, M.E., Van Schmus, W.R., Karlstrom, K.E., Mueller. P.A., and Kamenov, G.D., 2015, Mid-Continent Mesoproterozoic Granite-Rhyolite Provinces revisited: evidence from new SHRIMP U-Pb ages, zircon saturation temperatures, and Hf isotopic compositions: Precambrian Research Special Issue, v. 65, p. 286- 312

Buslov, M.M., De Grave, J., Bataleva, E.A.V., Batalev, V.Yu., 2006, Cenozoic tectonic and geodynamic evolution of the Kyrgyz Tien Shan Mountains: A review of geological, thermochronological and geophysical data: Journal of Asian Earth Sciences, v. 29, 205-214

Crowley, J.L., Schmitz, M.D., Bowring, S.A., Williams, M.L., and Karlstrom, K.E., 2006, U-Pb and Hf isotopic analysis of zircon in lower crustal xenoliths from the Navajo volcanic field: 1.4 Ga mafic magmatism and metamorphism beneath the Colorado Plateau: Contributions to Mineralogy and Petrology, doi: 10.1007/ a00410–006–0061-z

Daniel, C.G., and Pyle, J.M., 2006, Monazite-xenotime thermochronometry and Al2SiO5 reaction textures in the Picuris Range, northern New Mexico: New evidence for a 1450–1400 Ma orogenic event: Journal of Petrology, v. 47, no. 1, p. 97–118, doi:10.1093/petrology /egi069

Daniel, C.G., Pfeifer, L.S., Jones, J. V., McFarlane, C.M., 2013, Detrital zircon evidence for non-Laurentian provenance, Mesoproterozoic (ca. 1490-1450 Ma) deposition and orogenesis in a reconstructed orogenic belt, northern New Mexico, USA: Defining the Picuris orogeny: Geological Society of America Bulletin, v. 125, p. 1423–1441, doi: 10.1130/ B30804.1

Doe, M.F., Jones, J.V., Karlstrom, K.E, Thrane, K., Frei, D., Gherels, G., Pecha, M., 2012, Basin formation near the end of the 1.60-1.45 Ga tectonic gap in southern Laurentia: Mesoproterozic Hess Canyon Group of Arizona and implications for ca. 1.5 Ga supercontinent configurations: Lithosphere, v. 4, no. 1, p. 77-88, doi:10.1130/L160.1

Doe, M.F., Jones, J.V., Karlstrom, K.E, Dixon, B., Gehrels, G., Pecha, M., 2013, Using detrital zircon ages and Hf isotopes to identify 1.48–1.45 Ga sedimentary basins and fingerprint sources of exotic 1.6–1.5 Ga grains in southwestern Laurentia: Precambrian Research, v. 231, p. 409-421

Duebendorfer, E.M., Chamberlain, K.R., Heizler, M.T., 2006, Filling in the North American tectonic gap: 1.60-1.59 deformation and orogenesis in southern Wyoming, USA: Geology, v. 114, no. 1, p. 19-42

Duebendorfer, E.M., Williams, M.L., Chamberlain, K.R., 2015, Case for a temporally and spatially extended Mazatzal orogeny: Lithosphere, v. 7, no. 6, p. 603-610

Frost, C.D., and Frost, B.R., 2010, On Ferroan (A-type) Granitoids: their Compositional Variability and Modes of Origin: Journal of Petrology, v. 52, i. 1, p. 39-53

Gaft, M., Nagili, L., Panczer, G., Rossman, G.R., Reisfeld, R., 2011, Laser-induced time-resolved luminescence of orange kyanite Al2SiO5: Optical Materials, v. 33, no. 10, p. 1476-1480

Gaston, L, 2006, $^{40}Ar/^{39}Ar$ muscovite thermochronology and geochronology of New Mexico pegmatites [M.S. thesis]: Socorro, New Mexico Institute of Mining and Technology, p. 139

Gonzales, D.A., Karlstrom, K.E., Siek, S., 1996, Syncontractional crustal anatexis and deformation during emplacement of ~1435 Ma plutons, Western Needle Mountains, Colorado: The Journal of Geology, v. 104, no. 2, p. 215-233

Goodge, J.W., and Vervoort, J.D., 2006, Origin of Mesoproterozoic A-type granites in Laurentia: Hf isotope evidence: Earth and Planetary Science Letters, v. 243, p. 711–731, doi:10.1016/j.epsl.2006.01.040

Grambling, J.A., and Codding, D.B., 1982, Stratigraphic and structural relationships of multiply deformed Precambrian metamorphic rocks in the Rio Mora area, New Mexico: Geological Society of America Bulletin, v. 93, p. 127–137.

Haapala, I., Rämö, O.T., 1999, Rapakivi granites and related rocks: an introduction, In Precambrian Research, v. 95, no. 1–2, p. 1-7, doi.org/10.1016/S0301-9268(98)00124-7

Harrison, T.M., 1981, Diffusion of 40Ar in hornblende: Contributions to Mineralogy and Petrology, v. 78, p. 324-331, doi: 10.1007/BF00398927.

Harrison, T. M., Duncan, I., and McDougall, I., 1985, Diffusion of 40Ar in biotite: Temperature, pressure, and compositional effects: Geochimica et Cosmochimica Acta, v. 49, no. 2461–2468

Harrison, T.M., Celerier, J., Aikman, A.B., Hermann, J., and Heizler, M.T., 2009, Diffusion of 40Ar in muscovite: Geochimica et Cosmochimica Acta, v. 73, p. 1039-1051, doi: 10.1016/j.gca.2008.09.038

Holcombe, R.J., and Callender, J.F., 1982, Structural analysis and stratigraphic problems of Precambrian rocks of the Picuris Range, New Mexico: Geological Society of America Bulletin, v. 93, p. 138–149, doi:10.1130/0016 - 7606(1982)93<138:SAASPO>2.0.CO;2

Jessup, M.J., Karlstrom, K.E., Connelly, J., Williams, M.L., Livaccari, R., Tyson, A., and Rogers, S.A., 2005, Complex Proterozoic crustal assembly of southwestern North America in an arcuate subduction system: The Black Canyon of the Gunnison, southwestern Colorado, in Karlstrom, K.E., and Keller, G.R., eds., Lithospheric structure and evolution of the Rocky Mountains: American Geophysical Union Geophysical Monograph 154, p. 21–38

Jones, J.V., III, Daniel, C.G., Frei, D., and Thrain, K., 2011, Revised regional correlations and tectonic implications of Paleoproterozoic and Mesoproterozoic metasedimentary rocks in northern New Mexico, USA: New findings from detrital zircon studies of the Hondo Group, Vadito Group, and Marqueñas Formation: Geosphere, v. 7, no. 4, p. 974–991, doi:10.1130/GES00614.1

Karlstrom, K.E., Amato, J.M., Williams, M.L., Heizler, M., Shaw, C., Read, A., and Bauer, P., 2004, Proterozoic tectonic evolution of the New Mexico region: A

synthesis, in Mack, G.H., and Giles, K.A., eds., The Geology of New Mexico: A Geologic History: New Mexico Geological Society Special Publication 11, p. 1–34

Karlstrom, K. E., Williams, M. L., Heizler, M. T., Holland, M. E., Grambling, T. A., and Amato, J. M., 2015, U-Pb monazite and 40Ar/39Ar data supporting polyphase tectonism in the Manzano mountains: a record of both the Mazatzal (1.66-1.60 Ga) and Picuris (1.45 Ga) orogenies, in: Frey, Bonnie A.; Karlstrom, Karl E. ; Lucas, Spencer G.; Williams, Shannon; Ziegler, Kate; McLemore, Virginia; Ulmer-Scholle, Dana S., New Mexico Geological Society 67th Annual Fall Field Conference Guidebook: Geology of the Belen Area

Kay, R. W., and S. M. Kay, 1993, Delamination and delamination magmatism: Tectonophysics, v. 219, p. 177–189

Kopera, J., Williams, M. L. & Jercinovic, M. J., 2002, Age constraints on fabric reactivation in the Tusas Range, northern New Mexico using electron microprobe monazite geochronology: Implications for the nature of regional 1.4 Ga deformation: Geological Society of America, Abstracts with Programs v. 34, i. 6, p. 180

Lanzirotti, A., and Hanson, G.N., 1997, An assessment of the utility of staurolite in U-Pb dating of metamorphism: Contributions to Mineralogy and Petrology, v. 129, no. 4, p. 352-365

Mako, C.A., Williams, M.L., Karlstrom, K.E., Doe, M.F., Powicki, D., Holland, M., Gehrels, G., and Pecha, M., 2015, Polyphase Proterozoic deformation in the Four

Peaks area, central Arizona, and relevance for the Mazatzal orogeny: Geosphere, v. 11, p. 1975-1995

Marshall, E.W., Lassiter, J. C., Barnes, J.D., Luguet, A., and Lissner, M., 2017, Mantle melt production during the 1.4 Ga Laurentian magmatic event: Isotopic constraints from Colorado Plateau mantle xenoliths: Geology, v. 45, no. 6, p. 519-522, doi:10.1130/G38891.1

Metcalf, R.V., 1990, Proterozoic geology of the Santa Fe Range, northern New Mexico, in Bauer, P.W., Lucas, S.G., Mawer, C.K., McIntosh, W.C., eds., Tectonic Development of the Southern Sangre de Cristo Mountains, New Mexico, p. 179-187

North American Magnetic Anomaly Group, 2002, Digital North American magnetic anomaly map: U.S. Geological Survey Map Series, scale 1:10,000,000 (http://pubs. usgs.gov/sm/mag_map/)

Nielsen, K.C. and Scott, T.E., 1979, Precambrian deformational history of the Picuris Mountains, New Mexico: New Mexico Geological Society Guidebook, 30, p.113-120

Nyman, M.W., Karlstrom, K.E., Andronicos, C., Graubard, C.M., 1994, Mesoproterozoic contractional orogeny in western North America: Evidence from 1.4 Ga plutons: Geology, v.22, i.10, p. 901-904

Pedrick, J. N., Karlstrom, K. E., and Bowring, S. A., 1998, Reconciliation of conflicting tectonic models for Proterozoic rocks of northern New Mexico: Journal of Metamorphic Geology, v. 16, p. 687–707

Read , A., Karlstrom, K.E., Grambling, J.A., Bowring, S.A., Heizler, M., and Daniel, C., 1999, A mid-crustal cross section from the Rincon Range, northern New Mexico: Evidence for 1.68 Ga pluton-influenced tectonism and 1.4 Ga regional metamorphism: Rocky Mountain Geology, v. 34, p. 67-91

Roberts, N.M.W., Slagstad, T., Viola, G., 2015, The structural, metamorphic and magmatic evolution of Mesoproterozoic orogens: Precambrian Research, v. 265, p. 1-9

Ross, J.V., 1962, The folding of angular unconformities: The Journal of Geology, v. 70, no. 3, p. 294-308

Ross, G.M., and Eaton, D.W., 2002, Proterozoic tectonic accretion and growth of western Laurentia: results from Lithoprobe studies in northern Alberta: Canadian Journal of Geosciences, 2002, v. 39, i.3, p. 313-329

Shaw, C.A., Heizler, M.H., and Karlstrom, K.E., 2005, 40Ar/39Ar thermochronologic record of 1.45–1.35 Ga intracontinental tectonism in the southern Rocky Mountains: Interplay of conductive and advective heating with intracontinental deformation, in Karlstrom, K.E., and Keller, G.R., eds., The Rocky Mountain Region—An Evolving Lithosphere: American Geophysical Union Geophysical Monograph 154, p. 163–184

Thompson, A.G., Grambling, J.A., Karlstrom, K.E., Dallmeyer, R.D., 1996, Mesoproterozoic metamorphism and 40Ar/39Ar thermal history of the 1.4 Ga Priest Pluton, Manzano Mountains, New Mexico: The Journal of Geology, v. 104, no. 5, p. 583-598

Whitmeyer, S.J., and Karlstrom, K.E., 2007, Tectonic model for the Proterozoic growth of North America: Geosphere, v. 3, p. 220–259, doi:10.1130/GES00055.1.

Williams, M.L., Jercinovic, M.J., Terry, M.P., 1999, Age mapping and dating of monazite on the electron microprobe: Deconvoluting multistage tectonic histories: Geology, v. 27, no. 11, p. 1023-1026

Williams, M.L., and Jercinovic, M.J., 2002, Microprobe monazite geochronology: putting absolute time into microstructural analysis: Journal of Structural Geology, v. 24, no. 6-7, p. 1013-1028

Williams, M.L., Jercinovic, M.J., Goncalves, P., and Mahan, K., 2006, Format and philosophy for collecting, compiling, and reporting microprobe monazite ages: Chemical Geology, v. 225, no. 1-2, p. 1-15

Williams, M.L., Jercinovic, M.J., Mahan, K.H., and Dumond, G., 2017, Electron Microprobe Petrochronology: Reviews in Mineralogy & Geochemistry, v. 83, p 153-182

Appendices

Appendix 1: U/Th-Pb analyses of Rio Mora monazite

Run			Date (Ma)	1sig (Ma)
Un	28	RM25-m1-core-right (m3-real)	1488	7.8
Un	29	RM25-m1-rim-left (m3-real)	1505	13.3
Un	30	RM25-m6-core	1517	5.4
Un	32	RM25-m5-core-left	1473	6.2
Un	33	RM25-m5-out-core-right	1445	11.2
Un	34	RM25-m5-out-rim-right	1442	9.2
Un	35	RM25-m8-core	1502	5.5
Un	37	RM25-m1(real)-core-right	1478	5.7
Un	38	RM25-m1(real)-rim-left	1455	6.4
Un	39	RM25-m7-core-bot	1487	24.5
Un	40	RM25-m7-rim-top	1435	6.5
Un	41	RM25-m6-mid-out-core	1525	2.7
Un	42	RM25-m9-core	1523	2.6
Un	9	RM-23-m10-just-outside-core-left	1450	6.1
Un	10	RM-23-m10-low-Th-left	1447	6.4
Un	7	RM-23-m8-inner-rim-right	1443	6.9
Un	5	RM-23-m8-core-right	1441	5.6
Un	11	RM-23-m10-rim-left	1441	7
Un	4	RM-23-m1-high-Y-bot	1432	9.9
Un	6	RM-23-m8-rim-left	1430	6.3
Un	8	RM-23-m8-outer-rim-right	1424	4.5
Un	12	RM-23-m6-left	1422	6.4
Un	13	RM-23-m4-hi-Y-up-left	1417	5.1
Un	22	RM-22-m1 redo	1486	9.4
Un	23	RM-22-m2 redo	1469	6.3
Un	24	RM-22-m23 redo	1433	18.1
Un	25	RM-22-m4 redo	1488	8.8
Un	26	RM-22-m5 redo	1488	19.2

Appendix 2: Analytical data for $^{40}Ar/^{39}Ar$ analyses of Rio Mora samples

	ID	Power (Watts)	$^{40}Ar/^{39}Ar$	$^{37}Ar/^{39}Ar$	$^{36}Ar/^{39}Ar$ (x 10^{-3})	$^{39}Ar_K$ (x 10^{-15} mol)	K/Ca	$^{40}Ar^*$ (%)	^{39}Ar (%)	Age (Ma)	±1σ (Ma)
	DY18-RM-1, Hornblende, 4.93 mg, J=0.0039797±0.06%, IC=0.9980085±0.0005332, NM-300L, Lab#=66763-01, Helix MC										
X	A	1.5	282.9	4.602	574.8	0.2	0.11	40.1	2.1	683.9	18.6
X	B	2.0	232.6	5.385	503.1	0.1	0.095	36.3	3.1	531.6	31.8
X	C	2.5	210.8	15.41	167.3	0.1	0.033	77.2	4.2	921.8	42.1
X	D	3.0	251.2	21.68	76.23	0.1	0.024	91.8	5.9	1205.0	36.8
X	E	3.5	264.9	23.45	32.65	0.3	0.022	97.1	10.4	1305.8	14.0
X	F	4.0	278.4	24.40	15.69	0.9	0.021	99.1	22.0	1372.9	5.8
	G	4.5	282.1	24.29	10.79	1.5	0.021	99.6	40.9	1390.5	3.4
	H	5.0	285.2	24.76	11.27	1.2	0.021	99.6	56.4	1401.2	4.2
	I	5.5	282.2	24.88	11.41	0.8	0.021	99.5	67.5	1390.9	5.5
	J	6.0	285.2	25.47	9.565	0.8	0.020	99.8	77.9	1403.7	6.1
	K	6.5	285.4	25.10	8.414	1.1	0.020	99.9	92.3	1405.2	4.5
	L	7.0	289.2	25.55	9.381	0.4	0.020	99.8	97.0	1417.6	14.0
X	M	10.0	321.2	26.79	13.15	0.1	0.019	99.5	98.4	1521.8	47.9
X	N	15.0	337.7	26.79	15.46	0.1	0.019	99.3	100.0	1572.3	42.5
	Integrated age ± 2σ			n=14		7.7	0.021		K2O=0.15%	1369.2	4.9
	Plateau ± 2σ	steps G-L		n=6	MSWD=2.51	5.8			75.0	1397.6	6.3
	DY18-RM-12, Hornblende, 4.8 mg, J=0.0039818±0.08%, IC=0.9980085±0.0005332, NM-300L, Lab#=66765-01, Helix MC										
X	A	1.5	391.5	7.551	553.6	0.2	0.068	58.4	2.2	1189.2	20.6
X	B	2.0	207.3	13.60	215.1	0.1	0.038	69.9	3.2	840.1	34.9
X	C	2.5	157.5	16.32	44.88	0.1	0.031	92.4	4.7	844.8	23.9
X	D	3.0	197.6	17.54	23.58	0.3	0.029	97.2	7.5	1049.6	15.5
X	E	3.5	241.0	20.20	18.28	0.4	0.025	98.5	11.3	1230.5	13.9
	F	4.0	271.6	20.56	11.05	1.0	0.025	99.4	21.9	1350.3	4.7
	G	4.5	280.3	20.94	8.190	2.7	0.024	99.8	50.3	1384.3	2.0
	H	5.0	278.4	21.03	7.413	2.9	0.024	99.8	81.2	1378.3	1.7
X	I	5.5	266.7	21.24	8.814	1.0	0.024	99.7	91.5	1336.1	4.8
X	J	6.0	240.7	24.33	18.71	0.1	0.021	98.5	93.0	1232.7	30.5
X	K	6.5	253.5	27.22	17.18	0.1	0.019	98.9	93.8	1285.0	61.0
X	L	7.0	259.4	28.47	18.62	0.1	0.018	98.8	94.5	1306.3	79.0
X	M	10.0	213.3	24.23	24.78	0.1	0.021	97.5	95.8	1118.9	36.9
X	N	15.0	205.5	25.98	28.91	0.4	0.020	96.9	100.0	1083.6	9.7
	Integrated age ± 2σ			n=14		9.4	0.025		K2O=0.19%	1324.6	4.1
	Plateau ± 2σ	steps F-H		n=3	MSWD=22.11	6.6			69.9	1378.7	11.8
	DY18-RM-18, Hornblende, 4.06 mg, J=0.0039781±0.04%, IC=0.9980085±0.0005332, NM-300L, Lab#=66762-01, Helix MC										
X	A	1.5	273.6	1.913	165.2	0.8	0.27	82.2	3.2	1171.2	5.0
X	B	2.0	183.6	3.859	22.55	0.8	0.13	96.5	6.2	979.0	4.8
X	C	2.5	245.7	6.535	12.61	1.1	0.078	98.7	10.6	1240.5	4.1
X	D	3.0	290.9	7.607	5.684	2.6	0.067	99.6	20.8	1409.1	2.1
	E	3.5	293.8	7.745	4.813	4.6	0.066	99.7	38.8	1420.0	1.2
X	F	4.0	289.0	7.752	4.038	4.8	0.066	99.8	57.7	1404.4	1.2
X	G	4.5	284.6	7.727	4.429	2.9	0.066	99.8	69.2	1389.1	1.8
X	H	5.0	283.2	7.647	4.291	1.6	0.067	99.8	75.5	1384.2	3.2
X	I	5.5	276.8	7.581	4.179	1.0	0.067	99.8	79.6	1362.3	4.9
X	J	6.0	283.5	7.534	3.881	1.3	0.068	99.8	84.6	1385.4	3.9
X	K	6.5	256.1	7.071	4.753	0.6	0.072	99.7	86.8	1287.6	8.6

X	L	7.0	242.1	6.314	4.062	0.5	0.081	99.7	88.6	1236.2	9.9
X	M	10.0	249.4	6.535	4.636	1.3	0.078	99.7	93.8	1262.9	3.6
X	N	15.0	264.7	7.670	5.769	1.6	0.067	99.6	100.0	1318.1	3.2
	Integrated age ± 2σ			n=14		25.5	0.070		K2O=0.61%	1358.6	1.7
	Step E		steps E-E	n=1		4.592			18.0	1420.0	1.2

DY18-RM-18A, Hornblende, 3.66 mg, J=0.0039764±0.03%, IC=0.9980085±0.0005332, NM-300L, Lab#=66761-01, Helix MC

X	A	1.5	193.8	1.715	144.2	1.3	0.30	78.1	5.3	863.3	2.7
X	B	2.0	149.0	2.837	28.48	1.1	0.18	94.5	9.7	815.4	3.3
X	C	2.5	192.6	5.722	12.27	1.3	0.089	98.4	15.1	1031.2	2.9
X	D	3.0	265.7	7.357	7.440	2.6	0.069	99.4	25.9	1319.0	2.0
	E	3.5	278.3	7.457	5.646	4.2	0.068	99.6	43.0	1365.4	1.4
X	F	4.0	274.1	7.350	5.751	3.7	0.069	99.6	58.0	1350.4	1.4
X	G	4.5	270.8	7.337	5.775	2.7	0.070	99.6	69.1	1338.7	2.0
X	H	5.0	249.0	6.941	6.124	1.2	0.074	99.5	74.2	1259.8	3.8
X	I	5.5	247.6	6.718	5.655	1.1	0.076	99.6	78.7	1254.9	4.1
X	J	6.0	225.0	5.799	6.233	0.6	0.088	99.4	81.0	1168.0	7.9
X	K	6.5	216.8	5.218	6.321	0.4	0.098	99.3	82.7	1135.4	10.2
X	L	7.0	242.3	6.714	7.038	0.4	0.076	99.4	84.2	1233.7	13.6
X	M	10.0	269.3	7.762	8.176	1.7	0.066	99.3	91.3	1331.6	2.9
X	N	15.0	261.7	6.609	9.540	2.1	0.077	99.1	100.0	1301.9	2.4
	Integrated age ± 2σ			n=14		24.4	0.077		K2O=0.64%	1264.2	1.6
	Step E		steps E-E	n=1		4.180			17.1	1365.4	1.4

DY18-RM-2, Muscovite, .49 mg, J=0.0039997±0.09%, IC=0.9980085±0.0005332, NM-300L, Lab#=66766-01, Helix MC

X	A	0.8	152.4	0.0408	47.89	0.4	12.5	90.7	0.9	805.5	7.7
	B	1.3	291.4	0.0420	44.00	0.6	12.1	95.5	2.1	1370.0	8.8
	C	1.8	287.5	-0.0029	19.06	1.9	-	98.0	5.9	1381.8	2.6
	D	2.0	282.5	-0.0051	10.16	1.5	-	98.9	8.9	1373.7	3.3
	E	2.5	283.4	-0.0012	4.743	2.8	-	99.5	14.6	1382.2	1.9
	F	3.0	281.3	-0.0002	1.368	4.2	-	99.9	23.3	1378.6	1.4
	G	3.5	281.2	-0.0029	1.119	4.1	-	99.9	31.8	1378.4	1.3
	H	4.0	281.6	0.0089	0.9070	3.8	57.0	99.9	39.6	1380.0	1.4
	I	4.5	281.1	-0.0040	0.8619	4.3	-	99.9	48.5	1378.4	1.3
	J	5.0	280.6	0.0059	0.4686	4.6	87.0	100.0	57.9	1377.0	1.1
	K	5.5	279.7	0.0117	0.3391	3.8	43.5	100.0	65.8	1374.2	1.3
	L	6.0	279.6	-0.0169	0.2626	2.0	-	100.0	70.0	1373.7	2.6
	M	8.0	279.8	-0.0013	0.8420	2.3	-	99.9	74.8	1373.9	2.4
	N	10.0	280.1	-0.0003	0.9797	2.8	-	99.9	80.5	1374.6	1.8
	O	12.0	281.4	0.0056	0.3208	4.8	91.7	100.0	90.4	1380.0	1.2
	P	15.0	281.6	0.0173	0.2247	3.5	29.5	100.0	97.6	1380.5	1.6
	Q	20.0	281.0	-0.0011	0.7059	1.2	-	99.9	100.0	1378.2	4.5
	Integrated age ± 2σ			n=17		48.5	166.3		K2O=9.51%	1373.4	1.9
	Plateau ± 2σ		steps B-Q	n=16	MSWD=2.44	48.1			99.1	1378.0	2.1

DY18-RM-5, Muscovite, .82 mg, J=0.0039821±0.09%, IC=0.9980085±0.0005332, NM-300L, Lab#=66767-01, Helix MC

X	A	0.8	81.27	0.0296	14.15	1.9	17.2	94.9	2.0	490.1	1.2
X	B	1.3	159.8	0.0122	8.579	2.2	41.8	98.4	4.3	890.0	1.6
X	C	1.8	240.5	0.0183	2.664	5.3	28.0	99.7	9.9	1226.68	0.87
X	D	2.0	259.0	0.0105	1.494	4.8	48.6	99.8	15.0	1295.6	1.0
X	E	2.5	267.0	-0.0022	0.5317	7.7	-	99.9	23.1	1325.22	0.70
X	F	3.0	271.2	-0.0001	0.2681	10.7	-	100.0	34.3	1340.22	0.54
X	G	3.5	271.5	0.0007	0.3468	12.0	753.5	100.0	47.0	1341.27	0.49
X	H	4.0	269.4	-0.0012	0.3602	10.0	-	100.0	57.6	1333.81	0.57
X	I	4.5	268.9	0.0047	0.4278	7.5	107.7	100.0	65.5	1331.98	0.74

X	J	5.0	266.9	-0.0066	0.7484	4.2	-	99.9	69.9	1324.8	1.3
X	K	5.5	269.7	0.0012	0.6889	3.3	426.1	99.9	73.4	1334.6	1.5
X	L	6.0	271.9	0.0036	0.4663	3.2	140.7	99.9	76.8	1342.6	1.8
X	M	8.0	271.8	0.0015	0.4647	5.3	350.5	99.9	82.3	1342.16	0.95
X	N	10.0	274.1	-0.0023	0.2725	4.7	-	100.0	87.3	1350.5	1.1
X	O	12.0	275.3	0.0076	0.1623	4.0	67.3	100.0	91.5	1354.8	1.3
	P	15.0	275.8	0.0020	0.2987	3.1	256.8	100.0	94.8	1356.1	1.8
	Q	20.0	277.1	-0.0074	0.8752	2.4	-	99.9	97.3	1360.1	2.2
	R	30.0	277.2	0.0199	1.410	2.5	25.6	99.9	100.0	1360.1	2.0
	Integrated age ± 2σ			n=18		94.7	162.6		K2O=11.14%	1308.4	1.8
	Plateau ± 2σ	steps P-R		n=3	MSWD=1.49	8.010			8.5	1358.56	3.303

DY18-RM-23, Muscovite, .32 mg, J=0.0039815±0.10%, IC=0.9980085±0.0005332, NM-300L, Lab#=66768-01, Helix MC

X	A	0.8	71.93	1.401	36.92	0.0	0.36	85.0	0.1	399.1	75.2
X	B	1.5	204.7	0.0489	15.52	0.7	10.4	97.8	1.7	1072.7	5.6
X	C	2.0	261.8	0.0032	4.336	3.2	159.2	99.5	9.0	1302.5	1.7
X	D	2.5	273.9	0.0027	1.908	6.3	187.3	99.8	23.4	1347.93	0.83
X	E	3.0	278.1	-0.0008	0.2355	11.7	-	100.0	50.0	1364.23	0.53
X	F	3.5	277.5	-0.0030	0.2360	9.2	-	100.0	71.0	1362.01	0.65
X	G	4.0	273.5	0.0025	1.428	2.8	205.8	99.8	77.4	1347.1	1.8
X	H	4.5	274.8	-0.0139	1.701	2.0	-	99.8	81.9	1351.2	2.5
X	I	5.0	276.0	0.0008	0.6212	2.2	666.1	99.9	87.0	1356.6	2.3
X	J	5.5	275.1	0.0077	0.7319	0.9	66.6	99.9	88.9	1353.4	5.8
X	K	6.0	274.9	-0.0306	0.2555	0.6	-	100.0	90.4	1353.1	7.8
	L	8.0	278.0	-0.0037	0.3966	1.6	-	100.0	93.9	1363.7	3.3
	M	10.0	278.8	-0.0389	0.6834	0.8	-	99.9	95.7	1366.0	6.8
	N	12.0	280.6	0.0252	0.8024	1.0	20.2	99.9	97.9	1372.1	5.5
	O	15.0	277.3	-0.0421	-0.2424	0.4	-	100.0	98.8	1361.8	11.8
	P	30.0	282.0	0.0234	0.6232	0.5	21.8	99.9	100.0	1377.2	9.3
	Integrated age ± 2σ			n=16		43.9	512.3		K2O=13.25%	1349.7	2.1
	Plateau ± 2σ	steps L-P		n=5	MSWD=0.82	4.2			9.6	1366.5	5.2

Notes:

Isotopic ratios corrected for blank, radioactive decay, and mass discrimination, not corrected for interfering reactions.

Errors quoted for individual analyses include analytical error only, without interfering reaction or J uncertainties.

Integrated age calculated by summing isotopic measurements of all steps.

Integrated age error calculated by quadratically combining errors of isotopic measurements of all steps.

Plateau age is inverse-variance-weighted mean of selected steps.

Plateau age error is inverse-variance-weighted mean error (Taylor, 1982) times root MSWD where MSWD>1.

Plateau error is weighted error of Taylor (1982).

Isotopic abundances after Steiger and Jäger (1977).

x preceding sample ID denotes analyses excluded from plateau age calculations.

Weight percent K_2O calculated from ^{39}Ar signal, sample weight, and instrument sensitivity.

Ages calculated relative to FC-2 Fish Canyon Tuff sanidine interlaboratory standard at 28.201 Ma

Decay Constant (LambdaK (total)) = 5.463e-10/a

Correction factors:

$(^{39}Ar/^{37}Ar)_{Ca}$ = 0.000709 ± 0.000006

$(^{36}Ar/^{37}Ar)_{Ca}$ = 0.0002818 ± 0.0000005

$(^{38}Ar/^{39}Ar)_{K}$ = 0.01139±0.00003

$(^{40}Ar/^{39}Ar)_{K}$ = 0.006385 ± 0.0003

Appendix 3: Compiled $^{40}Ar/^{39}Ar$ thermochronologic ages for muscovite

Author	Sample Name	40Ar/39Ar Age (Ma)	1σ error (Ma)	Northing	Easting
Karlstrom et al. 2017					
	NK-94-64	1,437	5		
	NK-94-50B	1,438	5		
	NK-94-50B	1,461	6		
	NK-94-2A	1,398	6		
	NK-94-51	1,456	5		
Karlstrom et al. 2016					
	CB-48 (62019-01)	1,420	3		
	H-13-MAN-03	1,444	3		
Amato et al., 2011					
	03BM-108	1477	15	3614125	729672
	03BM-111	1472	9	3622904	728374
	04BM-150	1471	4	3591577	730381
	04BM-174	1467	13	3615870	730854
	03BM-112	1464	6	3621930	730257
	LORD-1	1463	5	3590962	708911
	NM-282-99	1463	4	3625851	731171
	NM-289-99	1462	5	3627606	722057
	LORD-2	1459	3	3590962	708911
	05BM-183	1451	4	3620936	732549
	NM-261-99	1448	3	3629088	729499
	NM-233-99	1441	3	3627606	722057
	03BM-117	1437	5	3620750	729689
	NM-141-98	1436	5	3624347	720346
	00BM-5	1431	6	3619690	727554
	LORD-3	1429	2	3590962	708911
	NM-109-98	1427	4	3623492	719310
	NM-234-99	1391	9	3627606	722057
Hodges et al., 1994					
	AZ85-5b	1412	5		
	AZ 203	1410	10		
Sanders et al., 2006					
	HP02-8	1264	10	3955088	462063
	HP02-8	1316	7	3955088	462063
	HP02-8	1314	11	3955088	462063
	LV02-3895	1284	2	3939144	489275

	LV02-3895	1268	2	3939144	489275
	LV02-3895	1286	3	3939144	489275
	EM02-1	1360	2	3959382	451917
	EM02-1	1376	2	3959382	451917
	EM02-1	1370	1	3959382	451917
	DCBZ01-3a	1365	2	3950939	432194
	ASF01-9	1372	2	3953775	419630
	RP87	1270	6		
	RP-34	1367	2		
	SFP	1362	2		
	SF21	1387	4		
	SF22	1336	3		
	SF23	1352	1		
	K01-SF	1266	6		
	SF3	1332	4		
Gaston 2014 (thesis)					
	2_1	1370		4033239	406803
	2_1	1367		4033239	406803
	B 2 1	1366		4033293	406818
	2 2	1378		4031855	409425
	B 2 2	1373		4031871	409425
	2 3	1373		4029700	408936
	B 2 3	1361		4029700	408936
	5 1	1376		4040930	405954
	5 2	1384		4040930	405954
	5 3	1378		4040930	405954
	2 4A	1374		4020339	405851
	2 4B	1368		4020339	405851
	2 4C1	1404		4020339	405851
	2 4C2	1403		4020339	405851
	2 4C3	1395		4020339	405851
	2 4C4	1399		4020339	405851
	B 01 01	1348		4040780	404078
	B 01 06	1366		4041371	407606
	B 02 02	1363		4041048	406376
	Bluebird	1381		4043551	405811
	Bluebird	1373		4043551	405811
	Bluebird	1369		4043551	405811
	Cribbenville	1356		4038165	407180
	LaJ	1384		4044377	405674
	LaP	1395		4036168	407802
	LaP	1392		4036168	407802
	Meadow	1354		4045475	405658
	P 01 01	1377		4040780	404078

P 01 01	1386	4040780	404078
P 01 01	1374	4040780	404078
P 02 01	1356	4040780	404078
P 01 02	1376	4041045	406371
P 02 02	1374	4041048	406376
P 02 02	1374	4041048	406376
P-01-03	1394	4041045	406371
P-01-03	1397	4041045	406371
P-01-04	1364	4041456	406331
P-01-04	1370	4041456	406331
P-01-05	1360	4041838	407508
P-01-05	1373	4041838	407508
P-01-06	1352	4041371	407606
P-01-06	1378	4041371	407606
P-01-06	1364	4041371	407606
Queen	1373	4040610	408128
Queen	1364	4040610	408128
Queen	1360	4040610	408128
Vestegard	1390	4038165	405811
Vestegard	1380	4038165	405811
2-7-17A	1438	3897858	364427
3-7-17A	1439	3897928	364485
4-7-17C	1433	3897245	364087
B-5-7-17-13	1432	3897245	364087
6-7-17A	1432	3886401	364620
7-7-17-13	1431	3881410	369644
8-7-17-13	1422	3881409	369700
9-7-17A	1438	3881327	369994
10-7-17-13	1408	3881327	369994
CB-48	1511	3874405	370643.4
KBP-99-3	1670	3846710	366853
KBP-99-8	1660	3846689	367175
H-13-MAN-02	1395	3820230	362542
H-13-MAN-03	1444	3820334	363635
KLP-156	1362	3802230	353122

Appendix 4: Compilation of U/Pb zircon ages of 1.4 Ga intrusions

Author	U/Pb Zircon Age	1σ error (Ma)	Lat.	Long.
Mako et al. 2015				
	1,449	13	33.705	-111.337
	1,437	15	33.684	-111.337
Moscati et al. 2017				
	1,451	13	38.761	-106.662
	1,425	12	39.302	-106.601
	1,434	6	39.011	-106.318
	1,439	11	38.856	-106.348
	1,435	15	39.26	-106.542
	1,415	15	39.108	-106.451
	1,436	11	38.994	-106.498
	1,436	14	38.605	-106.627
	1,419	14	39.119	-106.699
	1,429	9	39.036	-106.259
	1,414	20	38.924	-106.308
	1,441	54	38.987	-106.213
	1,438	11	38.92	-106.111
	1,436	8	38.891	-106.146
	1,434	6	38.815	-106.083
	1,435	26	39.167	-106.215
Holland et al. 2016				
	1,456	13	34.51	-106.441
	1,453	12	35.168	-106.438
Condie et al. 1999				
	1,406	13	36.869	-109.782
	1,412	20	37.131	-109.765
	1,435	15	37.003	-109.447
Gleason et al. 1994				
	1,427	27	34.731	-115.159
	1,416	17	34.731	-115.159
Bryant et al. 2001				
	1,418	2	34.412	-113.253
	1,410	4	34.454	-113.627
	1,414	4	34.279	-113.036
	1,414	4	34.454	-112.978
Crowley et al. 2006				
	1,418	1		
Amato et al. 2011				
	1470	16	32.715	-108.558
	1469	12	32.642	-108.542

	1463	8	32.635	-108.568
	1463	13	32.64	-108.551
	1463	13	32.491	-108.513
	1461	4	32.461	-108.576
	1459	14	32.72	-108.505
	1455	11	32.72	-108.505
Premo et al. UNPUB				
	1453	8	35.65	-112.86
	1438	9	35.729	-112.816
	1423	9	35.701	-112.845
	1422	12	35.719	-112.823
Jones et al. 2010				
*James Jones	1447	9	38.509	-106.327
	1437	5	38.895	-106.628
	1428	23	38.727	-106.763
Jessup et al. 2005				
	1434	2	38.532	-107.693
Tweto, 1987; Aleinikoff et al. 1993				
	1442	2	39.588	-105.644
Gonzales, 1996				
	1436	1	37.581	-107.799
	1442	3	37.494	-107.615
	1435	3	37.494	-107.615
	1438	9	37.494	-107.615
Bickford et al. 1989				
	1359	11	38.171	-105.293
	1423	28	38.904	-105.449
	1459	14	38.864	-105.392
	1441	82	38.168	-105.166
	1442	7	38.309	-105.259
	1439	8	38.315	-105.243
	1362	7	38.05	-105.007
	1371	14	38.059	-105.052
	1474	7	38.338	-105.704
	1460	21	38.371	-105.625
	1486	36	37.986	-105.123
Doe and Pearson, 1969				
	1420	40	39.3	-106.61
Aleinikoff 1983				
	1412	13	41.084	-106.228
Ferguson et al. 2004				
	1404	2	34.888	-113.972
Bryant and Wooden, 2008				

	1388	2	34.156	-113.853755
	1408	2	34.156	-113.853755
Frost et al, 1990				
	1439	7	41.1378	-106.985
Ramo et al. 2003				
	1461	24	32.756	-108.662
	1465	16	32.756	-108.662
Pedrick et al. 1998				
	1423	1	36.191	-105.511
Silver 1984				
	1460	10	35.786	-106.849
S.A. Bowring in Robertson and Condie 1989				
	1480	20	35.677	-105.697
Roths 1991				
	1462	67	32.453	-106.516
Kirby et al. 1995				
	1437	47	35.196	-106.457
Grambling et al., 1992				
	1430	20	36.488	-105.174
Crossey et al. 2016				
	1372	13	36.27	-114.194
Silver 1978				
	1425.4	25	31.504	-110.386
	1420	10	32.071	-110.104
Silver and McKinney 1962				
	1430	0	34.611	-115.578
Anderson 1989				
	1407	4	34.307	-114.345
	1401	5	34.303	-114.194
Silver et al. 1981				
	1411	3	34.615	-113.188
	1400	15	34.603	-112.409
	1440	20	33.423	-110.994
Anderson and Silver 1977				
	1440	15	30.97	-110.337
Daniel et al, 2013				
	1450	10	36.183	-105.79